UNIVERSITY OF KWAZULU-NATAL

Error Performance Analysis of Cross QAM and Space-Time Labeling Diversity for Cross QAM

Muhammad Wazeer Kamdar

Supervised By: Professor Hongjun Xu

Submitted in fulfilment of the degree of PhD in Engineering,
School of Engineering, University of KwaZulu-Natal, Durban, South Africa

November 2019

As the candidate's supervisor I agree to the submission of this thesis.

Date of Submission: _____

Supervisor Signature: _____

Professor Hongjun Xu

Declaration 1 - Plagiarism

I, Muhammad Wazeer Kamdar, declare that,

1. The research reported in this thesis, except where otherwise indicated, is my original work.

2. This thesis has not been submitted for any degree or examination at any other university.

3. This thesis does not contain other persons' data, pictures, graphs or other information, unless specifically acknowledged as being sourced from other persons.

4. This thesis does not contain other persons' writing, unless specifically acknowledged as being sourced from other researchers. Where other written sources have been quoted, then:

    a. Their words have been re-written but the general information attributed to them has been referenced;
    b. Where their exact words have been used, their writing has been placed inside quotation marks, and referenced.

5. This thesis does not contain text, graphics or tables copied and pasted from the Internet, unless specifically acknowledged, and the source being detailed in the thesis and in the References sections.

Signed: _____

Declaration 2 - Publications

DETAILS OF CONTRIBUTION TO PUBLICATIONS that form part and/or include research presented in this thesis (include publications in preparation, submitted, *in press* and published and give details of the contributions of each author to the experimental work and writing of each publication)

Publication 1:

Performance Analysis of Cross QAM with MRC over Dual Correlated Nakagami-m, -n, and -q Channels

Published by Wireless Personal Communications

Publication 2:

Performance Analysis of Cross QAM with MRC over Non-Identical Correlated Fading Channels

In preparation

Publication 3:

Uncoded Space-Time Labeling Diversity for Cross QAM with MPSK

In preparation

Signed: _____

Acknowledgements

Firstly, my gratitude and praise to the Almighty.

I would like to thank my supervisor, Professor Hongjun Xu, for the opportunity to study under him, and for his tutorage and assistance during this period. I would like to thank ARMSCOR for their funding of my research. I would like to also thank my family and friends for their support.

Abstract

This thesis contains three contributions to cross quadrature amplitude modulation (XQAM) systems. Paper A and paper B are concerning error performance analysis, and paper C involves the design of a space-time labeling diversity scheme for XQAM.

1) In paper A, an approximation of the symbol error probability (SEP) of a single-input multiple-output (SIMO) XQAM modulated system over dual correlated fading channels, including Rayleigh, Nakagami-m, Nakagami-n (Rice) and Nakagami-q (Hoyt), is derived. Diversity combining is achieved using maximal-ratio combining (MRC), and the moment generating function (MGF) is used to derive the average SEP equations. Tight approximations for the Gaussian Q-function and the generalized Gaussian Q-function are derived using the trapezoidal rule. The resulting expressions consist of a finite sum of MGF's which are accurate and easily evaluated. In addition, a transformation technique is used to convert the correlated channels into independent channels which are then used in the analysis. SEP simulation results show a tight match with the derived approximation expressions.

2) In paper B, the results from paper A are extended to consider an SIMO XQAM modulated system over an arbitrary number of non-identical, correlated fading channels. Rayleigh, Nakagami-m and Nakagami-q fading channels are considered. Diversity combining is achieved using MRC. The MGFs for the fading channels are used to obtain the average SEP. A transformation technique is proposed that uses knowledge of the channel covariance matrix to convert an arbitrary number of non-identical, correlated fading channels into independent channels, which are then used in the analysis. SEP simulation results are shown to match well with the theoretical results.

3) In paper C, an uncoded space-time labeling diversity (USTLD) system with improved bandwidth efficiency for XQAM is proposed. The proposed system is a combination of USTLD with XQAM and M-ary phase shift keying (MPSK) modulation. A low complexity detection scheme is proposed based on the maximum likelihood (ML) detection scheme. A simple approach is discussed to design mappers for XQAM and MPSK which are then used in the proposed system. Rayleigh flat-fading conditions are considered, and the tightness achieved by a theoretical average bit error probability (ABEP) bound is investigated. By introducing extra bits to a USTLD system via a 16-PSK phase component, the data rate for 32XQAM and 128XQAM USTLD can be improved by 20% and 14.3% respectively. Simulation

results show that the performance of the proposed system closely matches performance of the standard USTLD system at high SNR.

Contents

Part 2: Included Papers

Paper A

Paper B

List of figures

List of tables

List of acronyms

ABEP	Average Bit Error Probability
ADSL	Asymmetric Digital Subscriber Line
ASK	Amplitude Shift Keying
AWGN	Additive White Gaussian Noise
BER	Bit Error Rate
BICM-ID	Bit-Interleaved Coded Modulation with Iterative Decoding
DD	Direct Detection
DVB	Digital Video Broadcasting
EAST	Embedded Alamouti Space Time
EGA	Exhaustive Gaussian Approach
FSO	Free Space Optical
HARQ	Hybrid Automatic Repeat Request
HDRAC	High Data Rate Alamouti Codes
IID	Independent and Identically Distributed
LC	Low Complexity
LOS	Line of Sight
MGF	Moment-Generating Function
MIMO	Multiple-Input Multiple-Output
MISO	Multiple-Input Single-Output
ML	Maximum Likelihood
MRC	Maximal-Ratio Combining
OFDM	Orthogonal Frequency Division Multiplexing

PD	Product Distance
PDF	Probability Density Function
PSK	Phase Shift Keying
QAM	Quadrature Amplitude Modulation
SEP	Symbol Error Probability
SER	Symbol Error Rate
SIMO	Single-Input Multiple-Output
SISO	Single-Input Single-Output
SNR	Signal-to-Noise Ratio
SQAM	Square Quadrature Amplitude Modulation
SSD	Signal Space Diversity
STBC	Space-Time Block Code
STTC	Space-Time Trellis Code
SVD	Singular Value Decomposition
TCM	Trellis Coded Modulation
TQAM	Triangular Quadrature Amplitude Modulation
USTLD	Uncoded Space-Time Labeling Diversity
VDSL	Very High Speed Digital Subscriber Line
XQAM	Cross Quadrature Amplitude Modulation

Notation

$E[\cdot]$	Expectation
$(\cdot)^*$	Conjugate
$\text{argmin}_w(\cdot)$	Minimum of the argument with respect to w
$\text{argmax}_w(\cdot)$	Maximum of the argument with respect to w
$\text{Re}\{\cdot\}$	Real component of a complex argument
$\lvert\cdot\rvert$	Euclidean Norm
$\lVert\cdot\rVert_F$	Frobenius Norm
$(\cdot)^T$	Transpose
$(\cdot)^H$	Hermitian Transpose
$\Gamma(\cdot)$	Incomplete Gamma Function
$CN(\mu, \sigma^2)$	Complex Gaussian (normal) distribution with mean μ and variance σ^2
$I_0(\cdot)$	Modified Bessel function of the first kind with order zero

Part I

Introduction

1 Introduction

Wireless communication is an area of high interest nowadays and has applications in many different fields. There are ever increasing demands for high speed data communication over varying distances and channel conditions.

New transmission schemes and techniques are being researched to meet the symbol error rate (SER) or bit error rate (BER), system throughput and delay requirements for specific applications. Diversity techniques are one such method, and include space diversity, time diversity, frequency diversity, cooperative diversity, and more. Diversity schemes use multiple copies of the same information to improve the BER or SER of a system. In recent works, a promising new diversity scheme called uncoded space-time labeling diversity (USTLD) has been proposed.

The choice of modulation scheme for a system can have a significant effect on system error performance. Different modulation schemes exist in the literature. An important and widely used scheme is quadrature amplitude modulation (QAM). There are various different possible configurations of the QAM constellation, including square QAM (SQAM), rectangular QAM, triangular QAM (TQAM), and cross QAM (XQAM).

It is important to be able to predict the BER or SER performance of a wireless communication system to ensure that the system will meet the BER or SER requirements for a particular application. In aid of this, probability distributions are commonly used in modelling real-life fading channel conditions. Some commonly used distributions include Rayleigh, Nakagami-m, Nakagami-n (Rice) and Nakagami-q (Hoyt) distributions. Other aspects of the channel condition need to be considered as well in order to accurately predict the behaviour of a system. These include the effects of correlation between multiple fading channels, or channels that are not identically distributed.

1.1 Cross quadrature amplitude modulation

Digital QAM is a modulation scheme widely used in wireless communication. QAM consists of two carrier signals that are amplitude modulated. The carriers are also 90 degrees out of phase with each other (orthogonal), and are called quadrature carriers [1].

The most common configuration for a QAM constellation is square QAM, as this minimizes symbol error probability by maximizing the Euclidian distance between any two constellation points. However, this configuration can only be used when the number of bits to be transmitted is even: 4QAM for 2 bits, 16QAM for 4 bits, etc. Historically, rectangular QAM was used for systems that required the transmission of an odd number of bits: 8QAM for 3 bits, 32QAM for 5 bits, etc.

XQAM is an alternative configuration used in place of rectangular QAM for odd bit transmission. It was proven in [2] that using XQAM instead of rectangular QAM results in greater power efficiency and at least a 1dB signal-to-noise ratio (SNR) gain. Due to the benefits of the scheme, XQAM is used in adaptive modulation schemes as it allows for smaller steps in modulation size [3-7], in blind equalization [8], and is also used in various systems such as ADSL, VDSL and in DVB-C [9-11].

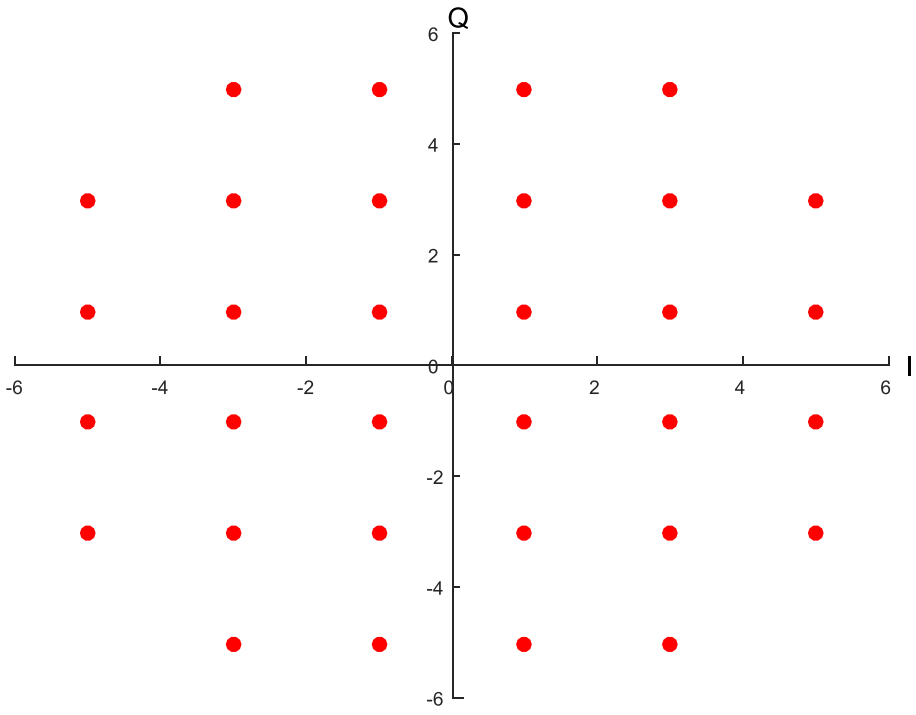

Fig. 1 32XQAM constellation diagram

1.2 Fading channel models

For SER or BER performance analysis, we need a mathematical model that approximates the behavior of a wireless fading channel. Covered here is a brief overview of the fading channel models relevant to this thesis, based on the material in [12] and [13].

1.2.1 Rayleigh

Rayleigh fading refers to a channel that experiences fading according to a Rayleigh distribution. This model is applicable to wireless systems without a dominant line of sight component, such as the scattered paths in tropospheric [14] and ionospheric [15-16] signal propagation. Other examples include propagation in heavily built up city centres [17] and the reflected and refracted paths in ship-to-ship radio links [18]. For Rayleigh fading, the probability density function (PDF) of the channel fading amplitude α is given by

$$p_\alpha(\alpha) = \frac{\alpha}{\sigma^2}\exp\left(-\frac{\alpha^2}{2\sigma^2}\right), \quad \alpha \geq 0 \tag{1}$$

where σ^2 is the channel variance.

1.2.2 Nakagami-n (Rician)

A channel experiencing Rician fading shows the characteristics of the Rician distribution. This model is applicable to systems where the signal arrives at the receiver via multiple paths, but at least one of the paths is dominant, typically a line of sight (LOS) component. This fading model is applicable to microcellular urban and suburban land–mobile [19], picocellular indoor [20], and factory [21] environments with LOS paths. It also applies to the dominant LOS path of satellite [22-23] and ship-to-ship [18] radio links. The PDF of the channel fading amplitude α for the Rician distribution is given by

$$p_\alpha(\alpha) = \frac{\alpha}{\sigma^2}\exp\left(-\frac{\alpha^2+s^2}{2\sigma^2}\right)\cdot I_0\left(\frac{\alpha s}{\sigma^2}\right) \tag{2}$$

where $I_0(\cdot)$ is the modified Bessel function of the first kind with zero order, and s^2 is the power of the LOS component, and σ^2 is the power in the remaining multipaths. We can define Rician fading in terms of two parameters: K represents the ratio of the power in the LOS component to the power in the other components:

$$K = \frac{s^2}{2\sigma^2} \tag{3}$$

and Ω represents the average fading power and is given by

$$\Omega = s^2 + 2\sigma^2 \tag{4}$$

From (5-7) we can write the PDF for Rician fading in terms of K and Ω as

$$p_\alpha(\alpha) = 2\alpha\frac{1+K}{\Omega}\exp\left(-K-\frac{1+K}{\Omega}\alpha^2\right)\cdot I_0\left(2\alpha\sqrt{\frac{K(1+K)}{\Omega}}\right) \tag{5}$$

With no LOS component ($K = 0$), Rician fading becomes Rayleigh fading.

1.2.3 Nakagami-m

Nakagami fading was originally developed empirically based on measurements, and provides a better estimation for the behaviour of certain wireless fading channels [24]. For example, Nakagami fading is used to model interference from multiple sources in a cellular system [25] or for urban radio multipath channels [26]. Other applications for the Nakagami-*m* distribution include land–mobile [27-29] and indoor–mobile [30] multipath propagation, as well as scintillating ionospheric radio links [31-34]. PDF of the channel fading amplitude α for Nakagami-m distribution is given by

$$p_{\alpha}(\alpha) = 2\alpha \frac{2m^m \alpha^{2m-1}}{\Omega^m \Gamma(\mathrm{m})} \exp\left(-\frac{\mathrm{m}\alpha^2}{\Omega}\right), \qquad \alpha \geq 0, \quad m \geq \frac{1}{2} \tag{6}$$

where m is the Nakagami-m fading parameter, $\Gamma(\cdot)$ is the incomplete gamma function, which is defined as $\Gamma(\alpha) = \int_0^{\infty} t^{\alpha-1} e^{-t} dt$ and Ω is the average fading power.

1.2.4 Nakagami-q (Hoyt)

The Nakagami-q (Hoyt) distribution is used in the modelling of certain systems affected by wireless fading [35-36]. It has found particular relevance to modelling cellular communications for satellite channels [36-38]. The PDF of the channel fading amplitude α for Nakagami-q distribution is given by

$$p_{\alpha}(\alpha) = \alpha \frac{(1+q^2)}{\mathrm{q}\Omega} \exp\left(-\frac{(1+q^2)^2}{4q^2\Omega}\alpha^2\right) \cdot I_0\left(\frac{\left(1-q^4\right)}{4q^2\Omega}\alpha^2\right), \qquad \alpha \geq 0,\ 0 \leq q \leq 1 \tag{7}$$

where q is the Nakagami fading parameter and Ω is the average fading power.

1.3 Signal-to-noise ratio

In analyzing the performance of a system, one of the most important metrics is the signal-to-noise ratio (SNR). As the name suggests, it's the ratio between the signal power and the noise experienced by the signal by the time it reaches the receiver. For error performance analysis, the average SNR is of interest, which is obtained by averaging the instantaneous SNR over the PDF of the fading distribution. This can be shown mathematically as [3, eq. 1.1]

$$\bar{\gamma} \triangleq \int_0^{\infty} \gamma p_{\gamma}(\gamma) d\gamma \tag{8}$$

where γ is the instantaneous SNR, and $p_\gamma(\gamma)$ is the PDF of the fading distribution in terms of γ. The PDF of the instantaneous SNR for the fading channels described above are given by [3, pg. 21]

Table 1 PDF of γ for selected fading channels

Fading channel	**PDF $p_\gamma(\gamma)$**
Rayleigh	$P_{\gamma_R}(\gamma) = \frac{1}{\bar{\gamma}}\exp\left(-\frac{\gamma}{\bar{\gamma}}\right)$
Nakagami-m	$P_{\gamma_m}(\gamma) = \frac{m^m \gamma^{m-1}}{\bar{\gamma}^m \Gamma(m)}\exp\left(-\frac{m}{\bar{\gamma}}\gamma\right), \quad m \geq \frac{1}{2}$
Nakagami-n	$P_{\gamma_n}(\gamma) = \frac{1+K}{\bar{\gamma}} e^{-K}\exp\left(-\frac{1+K}{\bar{\gamma}}\gamma\right) I_0\left(2\sqrt{\frac{1+K}{\bar{\gamma}}K\gamma}\right), \quad K \geq 0$
Nakagami-q	$P_{\gamma_q}(\gamma) = \frac{1+q^2}{2q\bar{\gamma}}\exp\left(-\frac{(1+q^2)^2}{4q^2\bar{\gamma}}\gamma\right) I_0\left(\frac{1-q^4}{4q^2\bar{\gamma}}\gamma\right), \quad 0 \leq q \leq 1,$

1.4 Moment generating function

The moment generating function (MGF) is a useful alternative representation of the probability distribution. The moment generating function, where it exists, can be found using the following equation [3, eq. 1.2]

$$M_\gamma(s) = \int_0^\infty p_\gamma(\gamma) e^{s\gamma} d\gamma \tag{9}$$

The MGF for the fading channels described above are given by [3, pg. 21].

Table 2 MGF of γ for selected fading channels

Fading channel	**MGF $M_\gamma(s)$**
Rayleigh	$M_{\gamma_R}(s) = (1+\bar{\gamma}s)^{-1}$
Nakagami-m	$M_{\gamma_m}(s) = (1+\frac{\bar{\gamma}}{m}s)^{-m}, \quad m \geq \frac{1}{2}$
Nakagami-n	$M_{\gamma_n}(s) = \frac{1+K}{1+K+\bar{\gamma}s}\exp\left(-\frac{K\bar{\gamma}s}{1+K+\bar{\gamma}s}\right), \quad K \geq 0,$
Nakagami-q	$M_{\gamma_q}(s) = \left(1+2\bar{\gamma}s+\left(\frac{2q\bar{\gamma}}{1+q^2}\right)^2 s^2\right)^{-\frac{1}{2}}, \quad 0 \leq q \leq 1$

1.5 Correlated fading

SER or BER performance analysis for diversity systems usually assumes independent fading for multiple paths at the receiver. However, there are many practical systems in which the fading for multiple paths is correlated.

Spatial correlation occurs due to insufficient antenna spacing [37-38], angle spread [39], or poor scattering conditions [40]. For example, small-size mobile units may have physical constraints that do not allow for sufficient antenna spacing. It is also possible for a system to undergo temporal correlation. This can be caused in time diversity schemes where there is imperfect interleaving (the channel symbols are not fully interleaved), or due to delay constraints [41-42].

Correlated fading affects the diversity gain of the system, and does not match the prediction obtained from assuming independent channels [43]. This issue was first explored in [44]. Correlated fading also has an effect on the channel capacity of a system. For example, [45] investigates the effect of correlated fading on the channel capacity of multi-element antenna systems.

1.6 Diversity schemes

A diversity technique is one that improves system error performance through redundancy: by having multiple copies of the information signal, the system is better able to recover the originally transmitted information. There are many diversity techniques, and more are still being researched. Below is a brief overview of diversity schemes relevant to this thesis:

1.6.1 Space Diversity

Space diversity is a method used to achieve either transmit diversity, receiver diversity or both transmit and receive diversity. Space diversity uses multiple antennas that are physically separated by a distance greater than half a wavelength at either transmitter, receiver or both transmitter and receiver [46-47]. This allows multiple copies of the transmitted signal to be received. Based on the number of transmit and receive antennas the transmission system can be classified into single-input single-output (SISO), single-input multiple-output (SIMO), multiple-input single-output (MISO), and multiple-input multiple-output (MIMO) which are illustrated in Fig. 2.

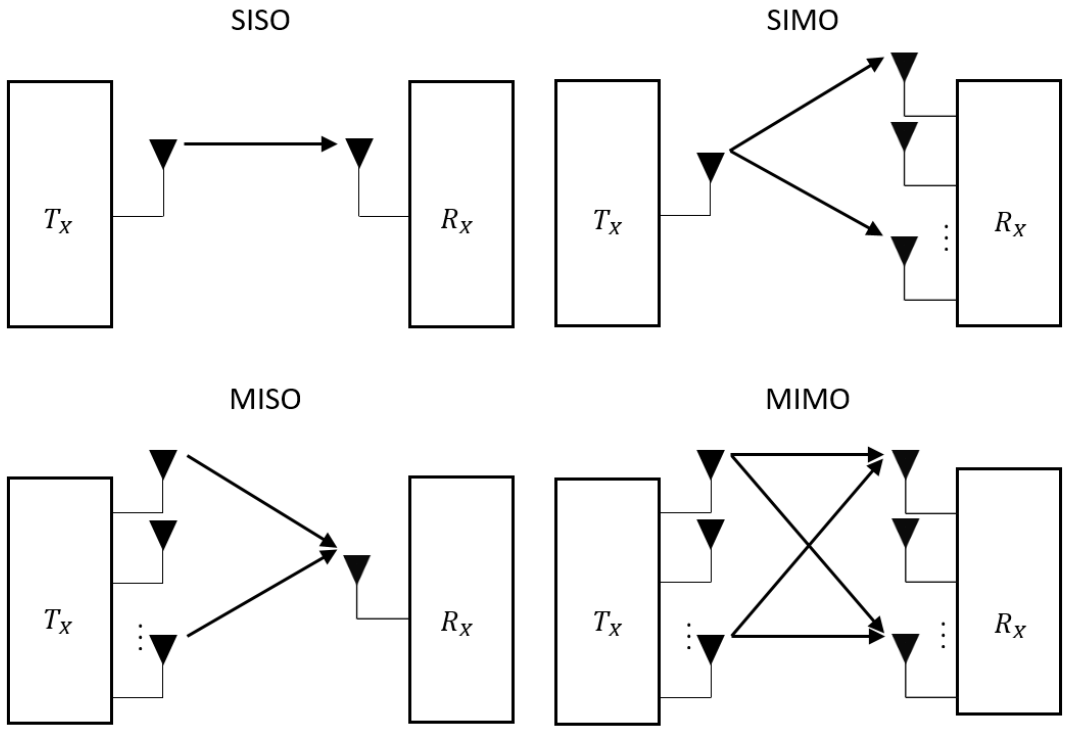

Fig. 2 SISO, SIMO, MISO and MIMO space diversity

1.6.2 Space-Time Diversity

Time diversity is achieved by transmitting multiple copies of the information signal over multiple timeslots. A space-time diversity scheme is one which utilizes both space and time diversity, such as space-time trellis codes (STTCs) or space-time block codes (STBCs).

1.6.3 Labeling Diversity

Labeling diversity is an emergent technology which uses multiple different bits-to-constellation signal mappers within the spatial streams at the transmitter. Recent research shows this to improve the performance of multi-antenna transmission systems [48].

1.7 Diversity Combining Schemes

In order to benefit from the diversity schemes in operation, the individual signals need to be combined at the receiver.

1.7.1 Maximal-ratio Combining

The optimal combining scheme at the receiver is maximal-ratio combining (MRC). In MRC, the signal from each receiver is multiplied by a weight factor that is proportional to the signal amplitude [49]. The signals are then added together. This causes the stronger signals to be amplified, weaker signals to be attenuated, and the received signal-to-noise ratio (SNR) to be maximized. MRC requires the knowledge of all channel parameters at the receiver.

Assuming the receiver has N_R antennas in SIMO system, the received signal is given by

$$\boldsymbol{y} = \sqrt{E_s}\boldsymbol{H}x + \boldsymbol{n} \tag{10}$$

where $\boldsymbol{y} = [y_1\ y_2\ \cdots\ y_{N_R}]^T$, x is the transmitted symbol, E_s is the transmit symbol power, $\boldsymbol{H} = [h_1\ h_2\ \cdots\ h_{N_R}]^T$ represents the channel fading, and $\boldsymbol{n} = [n_1\ n_2\ \cdots\ n_{N_R}]^T$ represents the additive white Gaussian noise (AWGN) with noise power N_0. Using MRC, the estimated signal $\hat{s}$ is given by [50]

$$\hat{s} = \frac{\sum_{i=1}^{N_r} h_i^* y_i}{\sqrt{E_s}\sum_{i=1}^{N_r}|h_i|^2} \tag{11}$$

where * represents conjugate operation.

For MRC, the combined conditional SNR is given by

$$\gamma_t = \sum_{i=1}^{N_r}\frac{E_s}{N_i}|h_i|^2 = \sum_{i=1}^{N_r}\gamma_i \tag{12}$$

2 Motivation and Research Objective

In [51], the exact average symbol error probability (SEP) of XQAM signal with MRC reception over independent, identically distributed Nakagami-m, -n and -q fading channels was analysed. However, correlation between fading channels was not considered. This motivates the derivation of expressions for SEP performance analysis of systems where it cannot be assumed that the fading channels are independent. The importance of considering correlated fading scenarios was discussed in Section 1.6.

Various approximations for the Gaussian Q-function and generalized Q-function were derived in [51] using numerical integration methods. However, the SEP expressions still include integral functions with exponential sums which are not analytical. This also motivates the derivation of approximation expressions that are in closed-form. In this thesis, the trapezoidal rule was used instead which produces closed-form expressions that also provide arbitrarily tight approximations for the Gaussian Q-function and generalized Gaussian Q-function.

In [52], a new diversity scheme called uncoded space-time labeling diversity was developed. Whilst the paper suggested design criterion for the signal mapper, it provided no practical method of finding an optimal mapper. It also only provided possible mappers for square-QAM systems. This motivates finding mappers for the modulation scheme of interest in this thesis i.e. XQAM. This new scheme also provides opportunity to find methods to develop new systems with improved error performance or spectral efficiency.

In the literature, analysis has been done for the SEP or BEP performance of various systems with specific detection, modulation and diversity schemes. An example is Digital Video Broadcasting-Cable (DVB-C), the details of which are found in [3]. The papers included in this thesis are contributions to this field, as they consider the case of a system using MRC detection, XQAM modulation, and either space or space-time diversity schemes.

3 Contributions of Included Papers

The work covered in this thesis has been detailed over three papers, which are presented in Part II. The details of the papers are summarized below.

Paper A

M.W. Kamdar and H. Xu, "SEP Performance Analysis of Cross QAM with MRC over Dual Correlated Nakagami-m, -n, and -q Channels," 2014.

An approximation of the symbol error probability (SEP) of a single-input multiple-output (SIMO) XQAM modulated system over dual correlated fading channels, including Rayleigh, Nakagami-m, Nakagami-n (Rice) and Nakagami-q (Hoyt), is derived. Diversity combining is achieved using maximal-ratio combining (MRC), and the moment generating function (MGF) is used to derive the average SEP equations. Arbitrarily tight approximations for the Gaussian Q-function and the generalized Gaussian Q-function are obtained from the numerical analysis technique; the trapezoidal rule. The resulting expressions consist of a finite sum of MGF's which are easily evaluated and accurate enough. In addition, a transformation technique is used to derive independent channels from the correlated channels which are then used in the analysis. The simulation results show a tight match with the derived approximation expressions.

Paper B

M.W. Kamdar and H. Xu, "SEP Performance Analysis of Cross QAM with MRC over Non-Identical Correlated Fading Channels," 2019.

An approximation expression is derived for the SEP of a single-input multiple-output (SIMO) XQAM modulated system over an arbitrary number of non-identical, correlated fading channels. Rayleigh, Nakagami-m and Nakagami-q fading channels are considered. SEP expressions for independent channels are derived using the MGFs for the fading channels, with MRC diversity combining. A transformation technique is proposed that uses knowledge of the channel covariance matrix to convert an arbitrary number of non-identical, correlated fading channels into identically distributed, independent channels. Simulations are performed in Matlab to verify the accuracy of the derived expressions.

Paper C

M.W. Kamdar, H. Xu and N. Pillay, “Uncoded Space-Time Labeling Diversity for Cross QAM with MPSK,” 2019.

An uncoded space-time labeling diversity (USTLD) system with improved bandwidth efficiency for XQAM is proposed. The proposed system is a combination of USTLD with XQAM and M-ary phase shift keying (MPSK) modulation. A low complexity detection scheme is proposed based on the maximum likelihood (ML) detection scheme. A simple approach is discussed to design mappers for XQAM and MPSK which are then used in the proposed system. Rayleigh flat-fading conditions are considered, and the tightness achieved by a theoretical average bit error probability (ABEP) bound is investigated. By introducing extra bits to a USTLD system via a 16-PSK phase component, the data rate for 32XQAM and 128XQAM USTLD can be improved by 20% and 14% respectively. Simulation results show that the performance of the proposed system closely matches performance of the standard USTLD system at high SNR.

4 Future Work

The derived expressions, whilst providing a very good approximation, are still not exact. Further research should be done into deriving exact closed-form expressions for the Q-function.

The expressions derived in paper A apply only to dual channel systems. Whilst Paper B's expression applies to systems of any order, it requires knowledge of the covariance matrix. There is still need for expressions to solve the problem of arbitrary order correlated fading channels where knowledge of the covariance matrix is not possible.

Using the MGF function, analysis has been performed over AWGN channels as well as Rayleigh, and various Nakagami channels (-m, -n and -q). There still remain other more generalized channel models that have not been considered. This includes Weibull, $\eta - \mu$ and $\kappa - \mu$ and log-normal shadowed fading, from which the channels considered can often be derived as special cases.

The papers presented in here focus only on SEP performance analysis. There are other performance metrics that can be considered as well, such as outage probability.

It is possible a better performing mapper design than that proposed in paper C exists, but it is yet to be proven. The error performance analysis expression provided only provides a bound on performance, an exact expression is yet to be derived.

5 References

[1] P. Rani and C. Budhiraja, "MIMO-OFDM Communication System Design using 256 HQAM," *IJARCSSE,* vol. 4, no. 9, pp. 558-563, Sep. 2014.

[2] J. Smith, "Odd-bit quadrature amplitude-shift keying," *IEEE Trans. on Commun.,* vol. 23, no. 3, pp. 385-389, 1975.

[3] S. Panigrahi and T. Le-Ngoc, "Fine-granularity loading schemes using adaptive Reed-Solomon coding for discrete multitone modulation systems," in *IEEE Int. Conf. on Commun.*, 2005.

[4] A. Ahrens and C. Lange, "Bit and Power Loading for Wireline Multicarrier Transmission Systems," *Transactions on Advanced Research,* vol. 2(1), pp. 3-9, 2006.

[5] M. Zwingelstein-Colin, M. Gazalet and M. Gharbi, "Non-iterative bit-loading algorithm for ADSL-type DMT applications," *IEE Proc. Commun.,* vol. 150, no. 6, pp. 414–418, 2003.

[6] M. Sternad and S. Falahati, "Maximizing throughput with adaptive MQAM based on imperfect channel predictions," in *IEEE PIMRC*, Barcelona, 2004.

[7] W. Wang, T. Ottosson, M. Sternad, A. Ahlen and A. Svensson, "Impact of multiuser diversity and channel variability on adaptive OFDM," in *IEEE Vehic. Technol. Conf.*, Orlando, FL, 2004.

[8] S. Abrar and I. Qureshi, "Blind equalization of cross-QAM signals," *IEEE Sig. Proc. Lett.,* vol. 13, no. 12, pp. 745-748, 2006.

[9] "ITU-T Std. G.992.1, Asymmetric digital subscriber line (ADSL) transceivers," 1999.

[10] "ITU-T Std. G.993.1, Very high speed digital subscriber line transceivers," 2004.

[11] "Digital Video Broadcasting (DVB); Framing Structure, Channel Coding and Modulation for Cable Systems," Apr. 1998. [Online]. Available: http://www.etsi.org/deliver/etsi_en/300400_300499/300429/01.02.01_60/en_300429v010201p.pdf.

[12] M. Simon and M.-S. Alouini, Digital Communication over Fading Channels, New York: Wiley-Interscience, 2005.

[13] J. Proakis, Digital Communications, New York: McGraw-Hill, 2001.

[14] H. Janes and P. Wells, "Some Tropospheric Scatter Propagation Measurements near the Radio Horizon," *Proc. IRE,* vol. 43, no. 10, pp. 1336-1340, Oct. 1955.

[15] G. R. Sugar, "Some Fading Characteristics of Regular VHF Ionospheric Propagation," *Proc. IRE,* vol. 43, no. 10, pp. 1432-1436, Oct. 1955.

[16] D. Chizhik, J. Ling, P. Wolniansky, R. Valenzuela, N. Costa and K. Huber, "Multiple-input-multiple-output measurements and modeling in Manhattan," *IEEE J. Select. Areas Commun.,* vol. 21, no. 3, pp. 321-331, Apr. 2003.

[17] S. e. a. Basu, "250 MHz/GHz Scintillation Parameters in the Equatorial, Polar, and Auroral Environments," *IEEE J. Select. Areas Commun.,* vol. 5, no. 2, pp. 102-115, Feb. 1987.

[18] T. L. Staley, R. C. North, W. H. Ku and J. R. Zeidler, "Performance of coherent MPSK on frequency selective slowly fading channels," in *Proc. IEEE Vehic. Technol. Conf.*, Atlanta, GA, Apr. 1996.

[19] K. A. Stewart, G. P. Labedz and K. Sohrabi, "Wideband channel measurements at 900 MHz," in *Proc. IEEE Vehic. Technol. Conf.*, Chicago, IL, Jul. 1995.

[20] R. J. C. Bultitude, S. A. Mahmoud and W. A. Sullivan, "A comparison of indoor radio propagation characteristics at 910 MHz and 1.75 GHz," *IEEE J. Select. Areas Commun.,* vol. 7, no. 1, pp. 20-30, Jan. 1989.

[21] T. S. Rappaport and C. D. McGillem, "UHF fading in factories," *IEEE J. Select Areas Commun.,* vol. 7, no. 1, pp. 40-48, Jan. 1989.

[22] G. H. Munro, "Scintillation of radio signals from satellites," *J. Geophys. Res.,* vol. 68, no. 7, pp. 1851-1860, Apr. 1963.

[23] P. D. Shaft, "On the Relationship Between Scintillation Index and Rician Fading," *IEEE Trans. Commun.,* vol. 22, no. 5, pp. 731-732, May 1974.

[24] A. Hottinen, O. Tirkkonen and R. Wichman, Multi-antenna Transceiver Techniques for 3G and Beyond, New York: Wiley, 2003.

[25] P. Vinothkumar and T. Dhaarani, "Estimating paper in variable gain relaying on imperfect CSI," *IJSRMS,* vol. 1, no. 1, pp. 26-32, 2014.

[26] Turin G., "Simulation of urban vehicle-monitoring systems," *IEEE Trans. Vehic. Technol.,* vol. 21, no. 1, pp. 9-16, Feb. 1972.

[27] H. Suzuki, "A Statistical Model for Urban Radio Propogation," *IEEE Trans. Vehic. Technol.,* vol. 25, no. 7, pp. 673-680, Jul. 1977.

[28] T. Aulin, "Characteristics of a digital mobile radio channel," *IEEE Trans. Vehic. Technol.,* vol. 30, no. 2, pp. 45-53, May 1981.

[29] W. R. Braun and U. Dersch, "A physical mobile radio channel model," *IEEE Trans. Vehic. Technol.,* vol. 40, no. 2, pp. 472-482, May 1991.

[30] A. U. Sheikh, M. Handforth and M. Abdi, "Indoor mobile radio channel at 946 MHz: Measurements and modeling," in *Proc. IEEE Vehic. Technol. Conf.*, Secaucus, NJ, May 1993.

[31] E. J. Fremouw and H. F. Bates, "Worldwide behavior of average VHF-UHF scintillation," *Radio Sci.,* vol. 6, no. 10, pp. 863-869, Oct. 1971.

[32] H. E. Whitney, J. Aarons, R. S. Allen and D. R. Seeman, "Estimation of the cumulative amplitude probability distribution function of ionospheric scintillations," *Radio Sci.,* vol. 7, no. 12, pp. 1095-1104, Dec. 1972.

[33] E. J. Fremouw, R. C. Livingston and D. A. Miller , "On the statistics of scintillating signals," *J. Atmos. Terr. Phys.,* vol. 42, no. 8, pp. 717-731, Aug. 1980.

[34] P. K. Banerjee, R. S. Dabas and B. M. Reddy, "C and L band transionospheric scintillation experiment: Some results for applications to satellite radio systems," *Radio Sci.,* vol. 27, no. 6, pp. 955-969, Nov. 1992.

[35] R. Hoyt, "Probablity functions for the modulus and angle of the normal complex variate," *Bell. Sys. Tech. J.,* vol. 26, no. 2, pp. 318-359, Apr. 1947.

[36] N. Youssef , W. Elbahri, M. Ptzold and S. Elasmi, "On the crossing statistics of phase processes and random FM noise in Nakagami-q mobile fading channels," *IEEE Trans. Wireless Commun.,* vol. 4, no. 1, pp. 24-29, Jan. 2005.

[37] R. Radaydeh, "Performance of cellular mobile systems employing SNR-based GSC in the presence of Rayleigh and Nakagami-q cochannel interferers," *IEEE Trans. Vehic. Technol.,* vol. 58, no. 6, pp. 3081-3088, Jul. 2009.

[38] N. Youssef , C.-X. Wang and M. Patzold, "A study on the second order statistics of Nakagami-Hoyt mobile fading channels," *IEEE Trans. Vehic. Technol.,,* vol. 54, no. 4, pp. 1259-1265, Jul. 2005.

[39] M. Saeed, B. Ali, S. Khatun and M. Ismail, "Impact of the Angular Spread and Antenna Spacing on the Capacity of Correlated MIMO Fading Channels," *IAJIT,* vol. 6, no. 1, pp. 60-65, Jan. 2009.

[40] M. Chiani, M. Win and A. Zanella, "On the Capacity of Spatially Correlated MIMO Rayleigh-Fading Channels," *IEEE Trans. Inform. Theory,* vol. 49, no. 10, pp. 2363-2371, Oct. 2003.

[41] K. Leeuwin-Boulle and J. Belfiore, "The cutoff rate of time correlated fading channels," *IEEE Trans. Inform. Theory,* vol. 39, no. 2, pp. 612-617, Mar. 1993.

[42] E. Baccarelli, "Performance bounds and cutoff rates for data channels affected by correlated randomly time-variant multipath fading," *IEEE Trans. Commun.,* vol. 46, no. 10, pp. 1258-1261, Oct. 1998.

[43] V. Veeravalli, "On Performance Analysis for Signaling on Correlated Fading Channels," *IEEE Trans. Commun.,* vol. 49, no. 11, pp. 1879–1883, Nov. 2001.

[44] J. Pierce and S. Stein, "Multiple diversity with nonindependent fading," *Proc. IRE,,* vol. 48, no. 1, pp. 89–104, Jan. 1960.

[45] D.-S. Shiu, G. Foschini, M. Gans and J. Kahn, "Fading correlation and its effect on the capacity of multi-element antenna systems," *IEEE Trans. Commun.,* vol. 48, no. 3, pp. 502–513, Mar. 2000.

[46] T. Rappaport, Wireless Communications: Principles and Practice, Singapore: Pearson Education, Inc., 2002.

[47] M. Krasicki, "Essence of 16-QAM labelling diversity," *Electron. Lett.,* vol. 49, no. 8, pp. 567-569, Apr. 2013.

[48] J. Salz and J. Winters, "Effect of fading correlation on adaptive arrays in digital mobile radio," *IEEE Trans. Vehic. Technol.,* vol. 43, no. 4, pp. 1049–1057, Nov. 1994.

[49] D. Malik and D. Batra, "Comparison of Various Detection Algorithms in a MIMO Wireless Communication Receiver," *IJECSE,* vol. 1, no. 3, pp. 1678-1685, 2012.

[50] D. Brennan, "Linear Diversity Combining Techniques," *Proc. IRE,* vol. 47, no. 6, pp. 1075–1102, Jun. 1959.

[51] H. Xu, K. Govindasamy and N. Pillay, "Uncoded space-time labeling diversity," *IEEE Comm. Lett.,* vol. 20, no. 8, pp. 1511-1514, June 2016.

[52] X.-C. Zhang, H. Yu and G. Wei, "Exact Symbol error probability of cross-QAM in AWGN and fading channels," *EURASIP J. Wirel. Commun. Netw.,* pp. 1–9, 2010.

Part 2

Included Papers

PAPER A

Published in: Wireless Personal Communications

Performance Analysis of Cross QAM with MRC over Dual Correlated Nakagami-m, -n, and -q Channels

Muhammad Wazeer Kamdar and Hongjun Xu

Abstract

An approximation of the symbol error probability (SEP) of a single-input multiple-output (SIMO) cross QAM (XQAM) modulated system over dual correlated fading channels, including Rayleigh, Nakagami-m, Nakagami-n (Rice) and Nakagami-q (Hoyt), is derived. Diversity combining is achieved using maximal-ratio combining (MRC), and the moment generating function (MGF) is used to derive the average SEP equations. Arbitrarily tight approximations for the Gaussian Q-function and the generalized Gaussian Q-function are obtained from the numerical analysis technique; the trapezoidal rule. The resulting expressions consist of a finite sum of MGF's which are easily evaluated and accurate enough. In addition, a transformation technique is used to derive independent channels from the correlated channels which are then used in the analysis. The simulation results show a tight match with the derived approximation expressions.

1 Introduction

Quadrature amplitude modulation (QAM) is a modulation scheme widely used in communication systems due to its bandwidth and power efficiency. Square QAM can be used when there is an even number of bits per symbol. However, when the number of bits per symbol is odd, it has been shown in [1] that greater power efficiency is achieved using cross QAM (XQAM) over square QAM. Due to this, XQAM has found use in adaptive modulation schemes as it allows for smaller steps in modulation size [2-6] and has been adopted in practical systems as well [7-9].

An important issue in the performance analysis of communication systems is the effects of the multipath fading channels. It has been shown in [10-11] that the received signals from different antennas can only be assumed to be statistically independent if the antennas are separated by a distance, generally larger than a half wavelength [11-12]. In systems where this condition is not met, the channel fading becomes correlated. Therefore, it is also important to consider the effects of correlation on the performance of diversity systems [12-16].

In [17], exact expressions in closed-form for the SEP of XQAM have been derived for the additive white Gaussian noise (AWGN) channel and independent fading channels. These expressions contain the Gaussian Q-functions and a finite number of numerically evaluable single integrals. In order to facilitate expression manipulations, much research has been done into trying to evaluate the Q-function, or to derive accurate approximations to the alternative Q-function. A summary of the latest research results in this field is found in [18].

Based on the work of [17], [18] analysed the average SEP of XQAM signal with maximal-ratio combining (MRC) reception over independent, but not necessarily identical, Rayleigh, Nakagami-m, Nakagami-n and Nakagami-q channels. The composite rectangular method and Simpson rule are both used to derive close approximations for the Q-function and generalized Q-function. The resulting approximate SEP expressions for the AWGN and fading channels are in the form of a sum of exponential functions and MGFs, respectively. SEP performance analysis of XQAM with MRC reception over generalized $\eta - \mu$ fading channels is also derived in [19]. However, the SEP expressions in [17-19] still include integral functions which are not analytical.

All the above performance analysis of XQAM has been only considered over independent fading channels. The assumption of statistical independence between the diversity channels is valid

only if they are sufficiently separated in space, in frequency or in time. However, there are many cases of practical interest where the assumption of statistical independence is not valid. The behaviour of the correlated channels affects the performance of the system. These effects need to be taken into consideration to gain a more accurate analysis of system performance. This paper extends the work of [17-19] to derive SEP performance of XQAM with MRC over dual correlated Nakagami-m, -n, and -q channels. Firstly, using the trapezoidal approximation rule the arbitrarily tight approximations of Q-function and the generalized Q-function are obtained, respectively. Secondly a transformation technique proposed in [20] is used to convert two correlated fading signals into two independent fading signals. And finally based on the moment generating function (MGF), approximations of the SEP over dual correlated fading channels are obtained in this paper.

The rest of the paper is organised as follows. Section 2 entails a description of the system model and all necessary parameters. In Section 3, approximate SEP expressions of XQAM in AWGN channel, single fading channel, dual independent fading channels and dual correlated fading channels are derived based on MGF, the trapezoidal approximation technique and the transformation technique. In Section 4, simulations are performed to test the accuracy and validity of the theoretical approximation expressions. Section 5 contains concluding remarks.

2 System model

A dual-branch single-input multiple-output (1×2 SIMO) system is taken into account in this paper. In the system model an $R = \log_2 M$ bit binary input is mapped according to an XQAM constellation as shown in [18]. We define the constellation size $M = 2^{2r+1}$ with $r \geq 2$ i.e. $M = 32, 128, 512, \cdots$. After mapping we obtain the transmit symbol x. This symbol x is then transmitted over the 1×2 SIMO Nakagami fading channels. The received signal is given by

$$\boldsymbol{y} = \sqrt{E_s}\boldsymbol{H}x + \boldsymbol{n} \tag{A. 1}$$

where $\boldsymbol{y} = [y_1\ y_2]^T$, x is the transmitted XQAM symbol with $E[|x|^2] = 1$. E_s is the transmit symbol power, $\boldsymbol{n} = [n_1\ n_2]^T$ is the complex additive white Gaussian noise (AWGN) with independent and identically distributed (IID) entries according to the complex Gaussian distribution with $CN(0,1)$. The amplitude $\boldsymbol{\alpha} = [\alpha_1\ \alpha_2]^T$ of fading channels $\boldsymbol{H} = [h_1\ h_2]^T$ including Rayleigh, Nakagami-*m*, Nakagami-*q* and Nakagami-*n*, are taken into account in this paper. $h_i = \left(h_i^I + jh_i^Q\right) + \left(h_D^{I_i} + jh_D^{Q_i}\right)$, $i \in [1\colon 2]$ where h_i^I and h_i^Q are Gaussian random variables with zero mean values, and $h_D^{I_i}$ and $h_D^{Q_i}$ are constant values. $h_D^{I_i} = 0$ and $h_D^{Q_i} = 0$ for Rayleigh, Nakagami-*m* and Nakagami-*q* channels while $h_D^{I_i} \neq 0$ and $h_D^{Q_i} \neq 0$ for Nakagami-*n* channel.

It is assumed that

$$E\left[h_i^I\right] = E\left[h_i^Q\right] = 0, \qquad i \in [1\colon 2] \tag{A. 2.1}$$

$$E\left[\left(h_i^I\right)^2\right] = E\left[\left(h_i^Q\right)^2\right] = \sigma^2, \qquad i \in [1\colon 2] \tag{A. 2.2}$$

$$E[h_i] = h_D^{I_i} + jh_D^{Q_i}, \qquad i \in [1\colon 2] \tag{A. 2.3}$$

$$E\left[h_i^I h_j^Q\right] = 0, \qquad i \in [1\colon 2];\ \ j \in [1\colon 2] \tag{A. 2.4}$$

$$C_{h_1^I h_2^I} = E[h_1^I h_2^I] = \rho\sigma^2 \tag{A. 2.5}$$

$$C_{h_1^Q h_2^Q} = E\left[h_1^Q h_2^Q\right] = \rho\sigma^2 \tag{A. 2.6}$$

where ρ is the correlation coefficient for dual fading channels. In Nakagami-n fading channels, parameter K is defined as the ratio of the power of the line of sight (specular) component to the average power of the scattered component [10]. K_i is given by

$$K_i = \frac{\left(h_D^{I_i}\right)^2 + \left(h_D^{Q_i}\right)^2}{2\sigma^2} \tag{A. 2.7}$$

Since the noise components are independent of the signal components and uncorrelated with each other, we have

$$E[n_1 n_2] = E\left[n_i h_k^I\right] = E\left[n_i h_k^Q\right] = 0 \qquad i \in [1:2]\,; k \in [1:2] \tag{A.2.8}$$

Consider a single channel, define $\gamma = \alpha^2 E_s/N_0$ as the instantaneous signal-to-noise ratio (SNR) at the receiver, where α is the channel's instantaneous fading amplitude. Then the probability density function (pdf) of the received instantaneous SNR γ over Rayleigh, Nakagami-*m*, Nakagami-*q* and Nakagami-*n* channels are given as, respectively, [18]

$$p_{\gamma_R}(\gamma) = \frac{1}{\bar{\gamma}} \exp\left(-\frac{\gamma}{\bar{\gamma}}\right) \tag{A.3}$$

$$p_{\gamma_m}(\gamma) = \frac{m^m \gamma^{m-1}}{\bar{\gamma}^m \Gamma(m)} \exp\left(-\frac{m}{\bar{\gamma}}\gamma\right), \qquad m \geq \frac{1}{2}, \tag{A.4}$$

$$p_{\gamma_q}(\gamma) = \frac{1+q^2}{2q\bar{\gamma}} \exp\left(-\frac{(1+q^2)^2}{4q^2\bar{\gamma}}\gamma\right) I_0\left(\frac{1-q^4}{4q^2\bar{\gamma}}\gamma\right), \qquad 0 \leq q \leq 1\,, \tag{A.5}$$

$$p_{\gamma_n}(\gamma) = \frac{1+K}{\bar{\gamma}} e^{-K} \exp\left(-\frac{1+K}{\bar{\gamma}}\gamma\right) I_0\left(2\sqrt{\frac{1+K}{\bar{\gamma}}K\gamma}\right), \qquad K \geq 0, \tag{A.6}$$

where $I_0(\cdot)$ is the modified Bessel function of the first kind and order zero, and $\Gamma(\cdot)$ is the incomplete Gamma function. m, q and K are parameters for Nakagami-*m*, Nakagami-*q* and Nakagami-*n*, respectively. $\bar{\gamma} = E\{\gamma\}$ is the average SNR at the receiver, where $\bar{\gamma} = 2\sigma^2 \frac{E_s}{N_0}$ is for Rayleigh, Nakagami-*m* and Nakagami-*q* channels while $\bar{\gamma} = (1+K)\frac{E_s}{N_0}$ for Nakagami-n fading channels.

By defining the moment generating function (MGF) as $M_\gamma(s) \triangleq E\{e^{-s\gamma}\}$. The MGFs corresponding to (A.3-A.6) are given as follows, respectively, [11]

$$M_{\gamma_R}(s) = (1 + \bar{\gamma}s)^{-1} \tag{A.7}$$

$$M_{\gamma_m}(s) = \left(1 + \frac{\bar{\gamma}}{m}s\right)^{-m}, \qquad m \geq \frac{1}{2} \tag{A.8}$$

$$M_{\gamma_q}(s) = \left(1 + 2\bar{\gamma}s + \left(\frac{2q\bar{\gamma}}{1+q^2}\right)^2 s^2\right)^{-\frac{1}{2}}, \qquad 0 \leq q \leq 1 \tag{A.9}$$

$$M_{\gamma_n}(s) = \frac{1+K}{1+K+\bar{\gamma}s} \exp\left(-\frac{K\bar{\gamma}s}{1+K+\bar{\gamma}s}\right), \qquad K \geq 0, \tag{A.10}$$

3 Average SEP of Cross QAM over Dual Correlated Nakagami-m, -n, and –q Channels

3.1 Exact SEP expression over AWGN channels

The exact expression for the SEP of XQAM in the AWGN channel is given by [18]

$$P_s(\gamma) = g_1 Q\left(\sqrt{2A_0\gamma}\right) + \frac{4}{M} Q\left(\sqrt{2A_1\gamma}\right) - g_2 Q^2\left(\sqrt{2A_0\gamma}\right) - \frac{8}{M}\sum_{k=1}^{v-1} Q_a\left(\sqrt{2A_0\gamma}, \alpha_k\right)$$

$$-\frac{4}{M}\sum_{k=1}^{v-1} Q_a\left(\sqrt{2A_0\gamma}, \beta_k^+\right) + \frac{4}{M}\sum_{k=1}^{v-1} Q_a\left(\sqrt{2A_0\gamma}, \beta_k^-\right) \quad (A.11)$$

where γ is the signal-to-noise ratio (SNR) at the receiver, M is the constellation size, and

$$g_1 = 4 - \frac{6}{\sqrt{2M}} \quad (A.11.1)$$

$$g_2 = 4 - \frac{12}{\sqrt{2M}} + \frac{12}{M} \quad (A.11.2)$$

$$v = \frac{1}{8}\sqrt{2M} \quad (A.11.3)$$

$$A_0 = \frac{48}{31M-32} \quad (A.11.4)$$

$$A_k = 2k^2 A_0, k = 1,2,\cdots,v \quad (A.11.5)$$

$$\alpha_k = \arctan\left(\frac{1}{2k+1}\right), k = 1,\cdots,v-1 \quad (A.11.6)$$

$$\beta_k^- = \arctan\left(\frac{k}{k-1}\right), k = 2,\cdots,v \quad (A.11.7)$$

$$\beta_k^+ = \arctan\left(\frac{k}{k+1}\right), k = 1,\cdots,v-1 \quad (A.11.8)$$

$Q(x)$ is the Gaussian Q-function which is given by

$$Q(x) = \frac{1}{\sqrt{2\pi}}\int_x^\infty e^{-t^2/2} dt \quad (A.12)$$

and $Q_a(x,\varphi)$ is a well-known integral function related to different forms of 1-D and 2-D Gaussian Q-functions

$$Q_a(x,\varphi) = \frac{1}{\pi}\int_0^\varphi \exp\left(-\frac{x^2}{2\sin^2\theta}\right) d\theta, x \geq 0 \quad (A.13)$$

Note that, for $M = 32$, we have $v = 1$, and the last three terms of (A.11) reduce to 0.

3.2 SEP Approximation of XQAM in AWGN channel using trapezoidal approximation

Since (A.15) still includes integral Q functions and $Q_a(x,\varphi)$ functions, it is very difficult to derive a closed-form SEP expression in fading channels. Several schemes have been proposed to approximate the Q function, but not $Q_a(x,\varphi)$ function [20-21]. Only the scheme based on the trapezoidal rule can also be used to approximate $Q_a(x,\varphi)$ function [21]. In this subsection, we will use the trapezoidal rule to approximate both Q function and $Q_a(x,\varphi)$ function. The trapezoidal rule is given as

$$\int_a^b f(x)dx = \frac{b-a}{n}\left[\frac{f(a)+f(b)}{2} + \sum_{k=1}^{n-1} f\left(a + k\frac{b-a}{n}\right)\right] \quad (A.14)$$

where n is the maximum number of summations. An alternate definition of $Q(x)$ known as Craig's formula is given by (4.2) of [11] as

$$Q(x) = \frac{1}{\pi}\int_0^{\pi/2} \exp\left(-\frac{x^2}{2\sin^2(\theta)}\right) d\theta \quad (A.15)$$

If we apply the trapezoidal rule to (A.15), then we have

$$Q(x) = \frac{1}{2n}\left(\frac{e^{-\frac{x^2}{2}}}{2} + \sum_{p=1}^{n-1} \exp\left(-\frac{x^2}{2\sin^2(\theta_p)}\right)\right) \quad (A.16)$$

where $\theta_p = \frac{p\pi}{2n}$. $Q^2(x)$ is also given by (4.9) of [11] as

$$Q^2(x) = \frac{1}{\pi}\int_0^{\pi/4} \exp\left(-\frac{x^2}{2\sin^2(\theta)}\right) d\theta \quad (A.17)$$

If we apply the trapezoidal rule to (A.17), then we have

$$Q^2(x) = \frac{1}{4m}\left(\frac{e^{-x^2}}{2} + \sum_{p=1}^{m-1} \exp\left(-\frac{x^2}{2\sin^2(\vartheta_p)}\right)\right) \quad (A.18)$$

where $\vartheta_p = \frac{p\pi}{4m}$. In addition, if we apply the trapezoidal rule to $Q_a(x,\varphi)$ we also have

$$Q_a(x,\varphi) = \frac{1}{\pi} \times \frac{\varphi}{n}\left[\frac{\exp\left(-\frac{x^2}{2\sin^2(\varphi)}\right)}{2} + \sum_{p=1}^{n-1} \exp\left(-\frac{x^2}{2\sin^2(p\varphi/n)}\right)\right] \quad (A.19)$$

We can then write an equation for the approximated SEP of XQAM in an AWGN channel by rewriting (A.11), using the results of (A.16), and (A.18-A.19):

$$P_s(\gamma) = \frac{g_1 e^{-A_0\gamma} - g_2 e^{-2A_0\gamma}}{8m} + \frac{g_1}{4m}\sum_{p=1}^{2m-1} \exp\left(-\frac{2A_0\gamma}{2\sin^2(\vartheta_p)}\right) - \frac{g_2}{4m}\sum_{p=1}^{m-1} \exp\left(-\frac{2A_0\gamma}{2\sin^2(\vartheta_p)}\right)$$

$$+\frac{1}{mM}\left(\frac{e^{-A_1\gamma}}{2}+\sum_{p=1}^{2m-1}\exp\left(-\frac{2A_1\gamma}{2\sin^2(\vartheta_p)}\right)\right)$$

$$+\frac{8}{M\pi n}\sum_{k=1}^{v-1}\alpha_k\left[\frac{\exp\left(-\frac{A_0\gamma}{sin^2(\alpha_k)}\right)}{2}+\sum_{p=1}^{n-1}\exp\left(-\frac{A_0\gamma}{\sin^2(p\alpha_k/n)}\right)\right]$$

$$+\frac{4}{M\pi n}\sum_{k=1}^{v-1}\beta_k^{+}\left[\frac{\exp\left(-\frac{A_0\gamma}{\sin^2(\beta_k^{+})}\right)}{2}+\sum_{p=1}^{n-1}\exp\left(-\frac{A_0\gamma}{\sin^2(p\beta_k^{+}/n)}\right)\right]$$

$$+\frac{4}{M\pi n}\sum_{k=1}^{v-1}\beta_k^{-}\left[\frac{\exp\left(-\frac{A_0\gamma}{\sin^2(\beta_k^{-})}\right)}{2}+\sum_{p=1}^{n-1}\exp\left(-\frac{A_0\gamma}{\sin^2(p\beta_k^{-}/n)}\right)\right] \quad \text{(A. 20)}$$

3.3 Approximated SEP of XQAM in single fading channel using MGF method

We can further derive the SEP of XQAM over a fading channel by averaging the approximated SEP expression derived in (A.20) over the fading distribution of the received SNR, γ, which is given by

$$P_s=\int_0^{\infty}P_s(\gamma)p_\gamma(\gamma)\,d\gamma \quad \text{(A. 21)}$$

Based on the definition of the MGF equation $M_\gamma(s)=\int_0^{\infty}\exp(-s\gamma)p_y(\gamma)d\gamma$, we can write the SEP expression (A.21) in a fading channel in terms of the MGF function as:

$$P_S(\bar{\gamma})=\frac{g_1}{8m}\cdot M_\gamma(-A_o)-\frac{g_2}{8m}\cdot M_\gamma(-2A_o)+\frac{g_1}{4m}\cdot\sum_{p=1}^{m-1}M_\gamma\left(\frac{-A_o}{\sin^2(\theta_p)}\right)$$

$$-\frac{g_2}{4m}\cdot\sum_{p=1}^{m-1}M_\gamma\left(\frac{-A_o}{\sin^2(\theta_p)}\right)+\frac{1}{2mM}\cdot M_\gamma(-A_1)+\frac{1}{mM}\cdot\sum_{p=1}^{2m-1}M_\gamma\left(\frac{-A_1}{\sin^2(\theta_p)}\right)$$

$$+\frac{4}{M\pi n}\cdot\sum_{k=1}^{v-1}\alpha_k\cdot M_\gamma\left(\frac{-A_o}{\sin^2(\alpha_k)}\right)+\frac{8}{M\pi n}\cdot\sum_{k=1}^{v-1}\alpha_k\cdot\left(\sum_{p=1}^{n-1}M_\gamma\left(\frac{-A_o}{\sin^2\left(\frac{p\alpha_k}{n}\right)}\right)\right)$$

$$+\frac{4}{M\pi n}\cdot\sum_{k=1}^{v-1}\beta_k^{-}\left[\frac{1}{2}\cdot M_\gamma\left(\frac{-A_o}{\sin^2(\beta_k^{-})}\right)+\sum_{p=1}^{n-1}M_\gamma\left(\frac{-A_o}{\sin^2\left(\frac{p\beta_k^{-}}{n}\right)}\right)\right]$$

$$-\frac{4}{M\pi n}\cdot\sum_{k=1}^{v-1}\beta_k^{+}\left[\frac{1}{2}\cdot M_\gamma\left(\frac{-A_o}{\sin^2(\beta_k^{+})}\right)+\sum_{p=1}^{n-1}M_\gamma\left(\frac{-A_o}{\sin^2\left(\frac{p\beta_k^{+}}{n}\right)}\right)\right] \quad \text{(A. 22)}$$

Note that $p_\gamma(\gamma)$ in (A.21) can be $p_{\gamma_R}(\gamma)$, $p_{\gamma_m}(\gamma)$, $p_{\gamma_{q_l}}(\gamma)$, or $p_{\gamma_{n_l}}(\gamma)$ in (A.3) to (A.6) and $M_\gamma(s)$ in (A.22) can be $M_{\gamma_R}(s)$, $M_{\gamma_m}(s)$, $M_{\gamma_{q_l}}(s)$, or $M_{\gamma_{n_l}}(s)$ in (A.7) to (A.10) to represent the symbol transmitted over Rayleigh, Nakagami-*m*, Nakagami-*q* or Nakagami-*n,* respectively.

3.4 Approximated SEP of XQAM over dual independent fading channels using MGF method

Since dual independent fading channels are assumed the PDF of the output instantaneous SNR of MRC combiner at the receiver is given by

$$p_\gamma(\gamma) = p_{\gamma_1}(\gamma_1)p_{\gamma_2}(\gamma_2) \tag{A.23}$$

where γ_i is the i'th path instantaneous SNR, $i \in 1,2$.

Then the MGF of γ becomes

$$\begin{aligned} M_\gamma(s) &= \int_0^\infty \int_0^\infty \exp[-s(\gamma_1+\gamma_2)]\, p_{\gamma_1}(\gamma_1)p_{\gamma_2}(\gamma_2)d\gamma_1\, d\gamma_2 \\ &= M_{\gamma_1}(s)M_{\gamma_2}(s) \end{aligned} \tag{A.24}$$

If dual fading channels are identically distributed then (A.24) becomes

$$M_\gamma(s) = \left(M_{\gamma_1}(s)\right)^2 \tag{A.25}$$

So, the SEP of XQAM over dual independent fading channels can be derived using (A.25) to replace $M_\gamma(s)$ in (A.22).

3.5 Approximated SEP of Cross QAM over dual correlated fading channels using MGF method

Several schemes have been proposed to derive SEP performance over correlated fading channels [22-25]. For dual correlated fading channels, the transformation approach proposed in [25] allows us to treat the correlated fading channels as two independent fading channels. Given two identically distributed but correlated fading channels with zero mean value, correlation coefficient ρ and average SNR $\bar{\gamma}_1 = \bar{\gamma}_2 = \bar{\gamma}$, we can generate two equivalent non-identically distributed independent fading channels with average SNR as follows:

$$\bar{\gamma}_1 = (1+\rho)\bar{\gamma} \tag{A.26}$$

$$\bar{\gamma}_2 = (1-\rho)\bar{\gamma} \tag{A.27}$$

Using the equivalent independent fading channels, we can express the MGF of γ as the product of the two diversity branches:

$$M_{\gamma}(s) = M_{\gamma_1}(s) M_{\gamma_2}(s) \tag{A.28}$$

Again, the SEP of XQAM over dual correlated fading channels can be derived using (A.28) to replace $M_{\gamma}(s)$ in (A.22). The above result is only for Rayleigh, Nakagami-m, and Nakagami-q fading channels, not for Nakagami-n fading channels. This is because the mean value of Nakagami-n fading is not zero. However, the transformation approach also allows us to convert dual correlated Nakagami-n channels into two independent fading channels. In general, given two identically distributed but correlated Nakagami-n fading channels with parameter K_1 and K_2, nonzero mean value, and correlation coefficient ρ, the transformation proposed in [25] also converts the dual correlated channels into two independent Nakagami-n fading channels with K_3 and K_4 which are given by

$$K_3 = \frac{(1+\beta)^2}{4(1+\rho)\sigma^2}\left[\left(h_D^{I_1}\right)^2 + \left(h_D^{Q_1}\right)^2\right] = \frac{(1+\beta)^2}{2(1+\rho)} K_1 \tag{A.29}$$

$$K_4 = \frac{(1-\beta)^2}{4(1-\rho)\sigma^2}\left[\left(h_D^{I_1}\right)^2 + \left(h_D^{Q_1}\right)^2\right] = \frac{(1-\beta)^2}{2(1-\rho)} K_1 \tag{A.30}$$

where β is defined as $\beta = h_D^{I_2}/h_D^{I_1}$ or $\beta = h_D^{Q_2}/h_D^{Q_1}$.

Specially when $\beta = 1$ the transformation converts dual correlated Nakagami-n fading channels with equal parameter $K_1 = K_2$ into two independent fading channels, one is Rayleigh fading channel ($K_4 = 0$), another is still Nakagami-n with parameter K_3 which is given by

$$K_3 = \frac{\left(h_D^{I_1}\right)^2 + \left(h_D^{Q_1}\right)^2}{(1+\rho)\sigma^2} = \frac{2}{1+\rho} K_1 \tag{A.31}$$

More detailed derivations and discussions are shown in the Appendix.

The average SNR $\bar{\gamma}_3$ and $\bar{\gamma}_4$ of h_3 and h_4 can be calculated as

$$\bar{\gamma}_3 = (1 + K_3)\frac{E_S}{N_0} \tag{A.32.1}$$

$$\bar{\gamma}_4 = (1 + K_4)\frac{E_S}{N_0} \tag{A.32.2}$$

Finally using the equivalent independent fading channel h_3 and h_4, we can express the MGF of γ as the product of the two diversity branches:

$$M_{\gamma}(s) = M_{\gamma_3}(s) M_{\gamma_4}(s) \tag{A.33}$$

4 Simulation Results

Monte Carlo simulations were performed in Matlab using 10^6 samples. The first simulations are performed over dual correlated fading channels to investigate how the levels of channel correlation affect the SEP performance of the system. 32-QAM and Rayleigh fading channel with $\sigma^2 = 0.5$ are used in these simulations. The degree of correlation between the channels is varied by adjusting the value of the correlation coefficient ρ**.** Fig. A1 shows dual Rayleigh channels with varying levels of correlation. Analytical results are also shown in Fig. A1. As the level of correlation between the two channels is increased, the system performance deteriorates. It is found that in order to achieve SEP rates below 10^{-3} for two highly correlated channels more than 10 dB increase in SNR is required compared to two uncorrelated channels. Fig. A1 also shows that analytical results match simulation results very well.

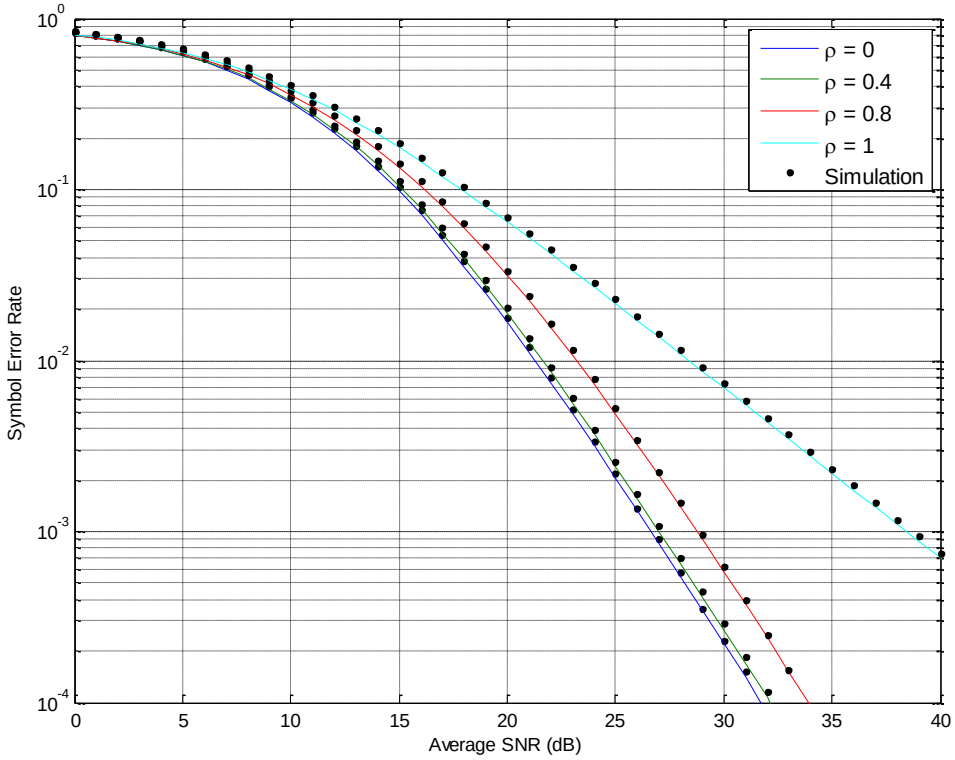

Fig. A.1 Dual Rayleigh channels with varying levels of correlation

The second simulations are performed to investigate the SEP performance over different dual correlated fading channels. The dual correlated fading channels are Rayleigh, Nakagami-m, Nakagami-n (Rician) and Nakagami-q (Hoyt) fading channels. The constellation size of XQAM was set to M = 32, 128 and 512, respectively**.** The following parameters were also used during simulations for Fig. A.2 to Fig. A.6: $\sigma^2 = 0.5$, correlation coefficient ρ is set to 0.4, Nakagami-m coefficient m is set to 3, Hoyt parameter Q is set to 0.6, and Trapezoidal parameter n is set to 10. For the Nakagami-n channel, Rician K factor is set to 3 for identically distributed channels. K_1 is then kept as 3 and K_2 is set to 4.5 for channels with different fading distributions. Simulation results are shown in Fig. A.2 to Fig. A.6 for Rayleigh, Nakagami-m, Nakagami-n (Rician) and Nakagami-q (Hoyt), respectively. Analytical results are also shown in Fig. A.2 to Fig. A.6. Again, all analytical results match simulation results very well.

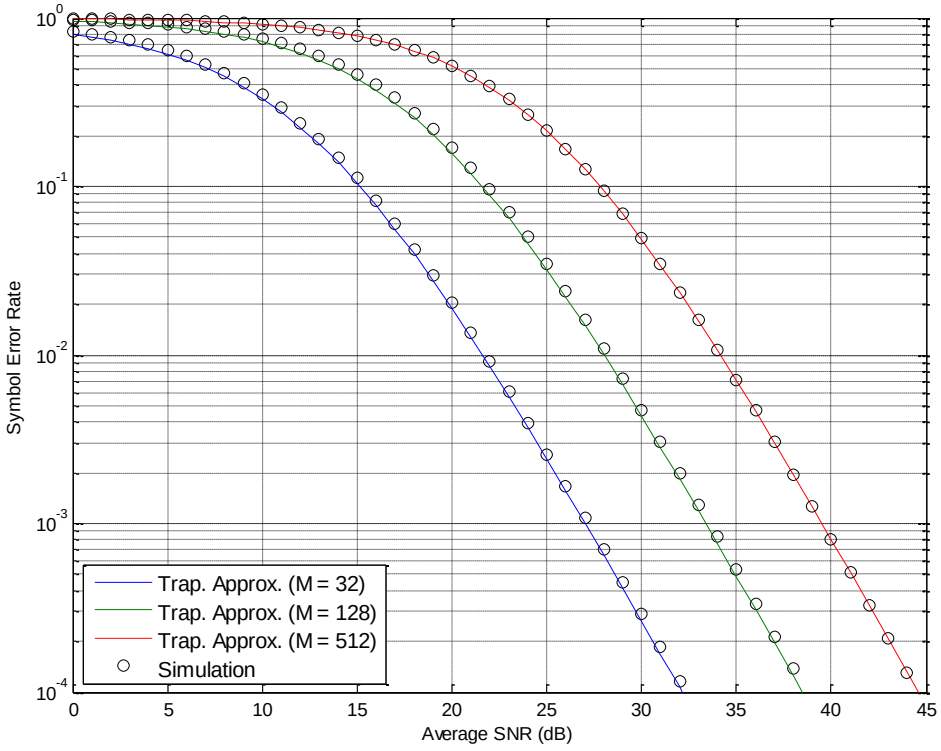

Fig. A.2 Rayleigh channels

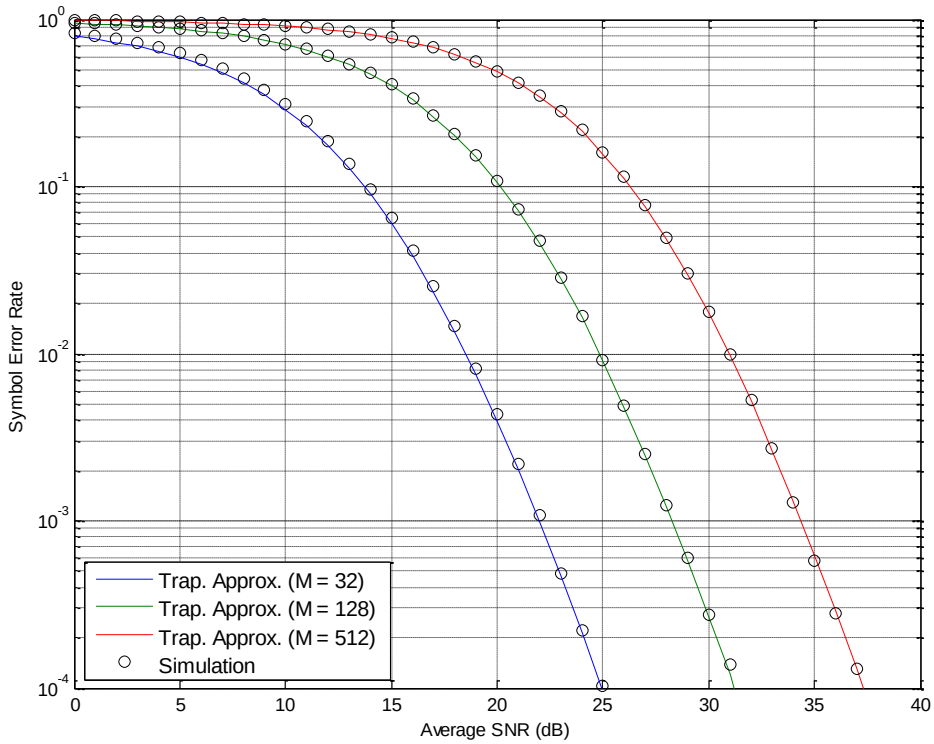

Fig. A.3 Nakagami-m channels with m = 3

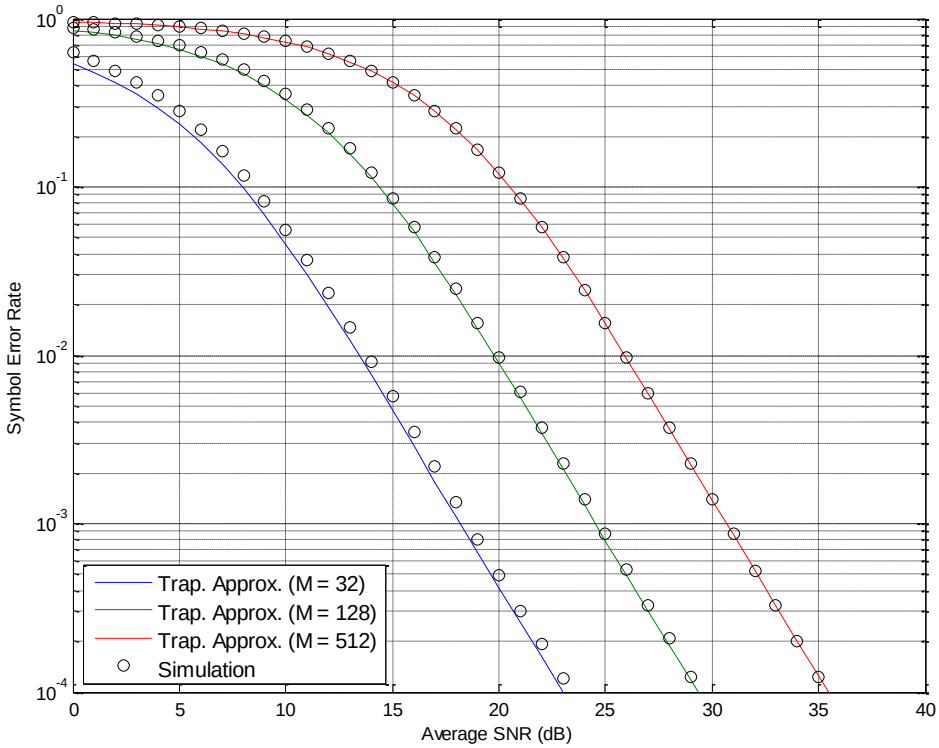

Fig. A.4 Rician channels with K_1=K_2 = 3

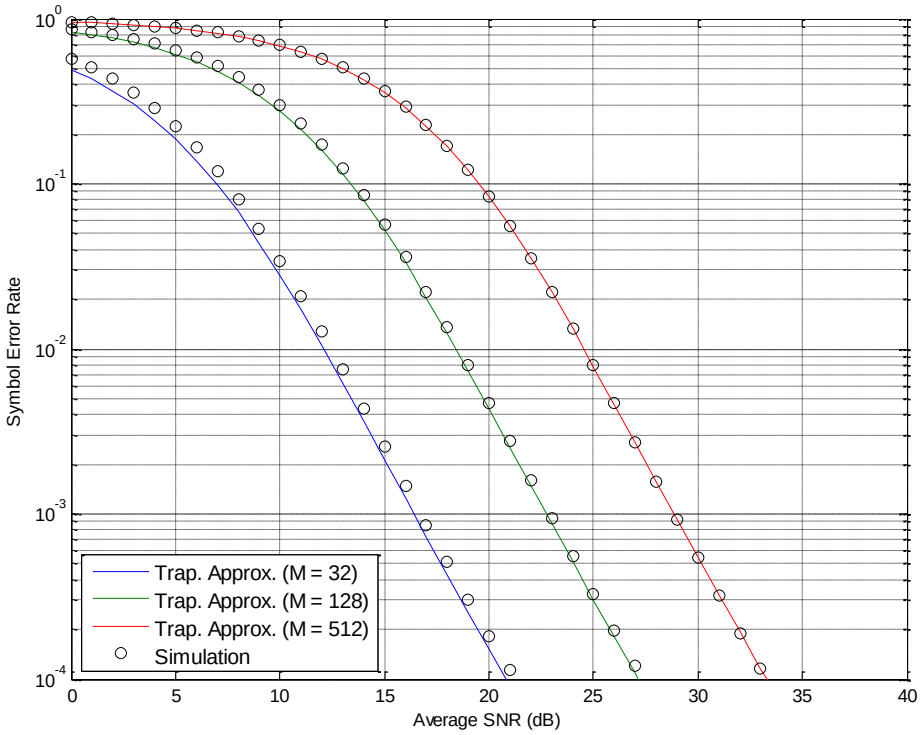

Fig. A.5 Rician channels with K_1=3, K_2=4.5

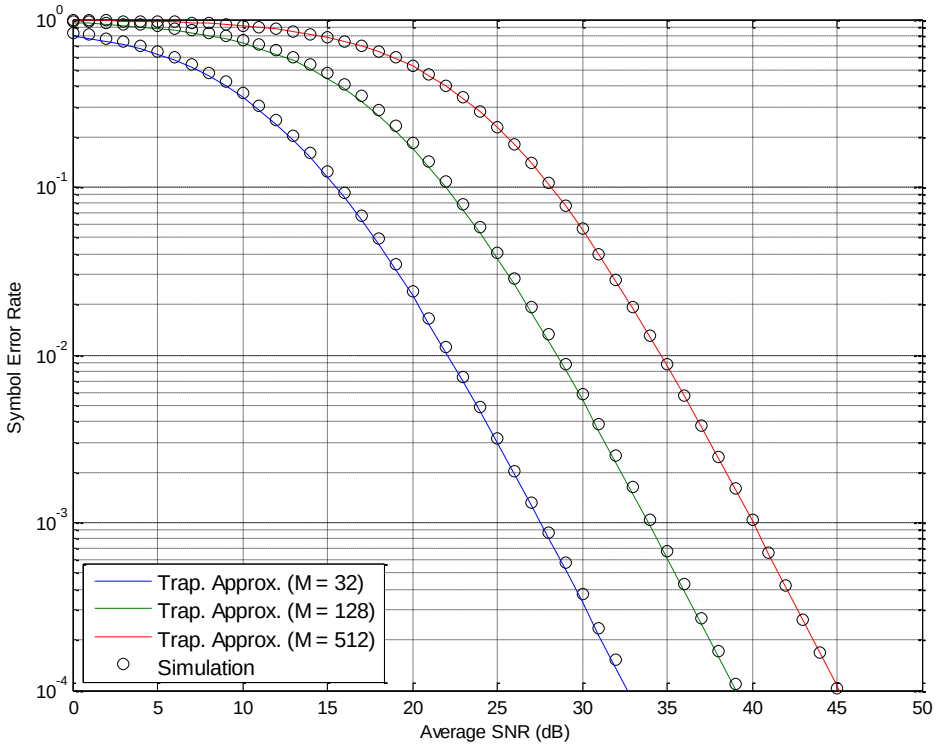

Fig. A.6 Hoyt channels with Q = 0.6

5 Conclusion

In this paper, the SEP of XQAM with MRC over dual correlated fading channels including Rayleigh, Nakagami-m, Rice and Hoyt channels has been derived based on the MGF method. A transformation technique is used to convert the dual correlated fading channels into two independent fading channels, which are then used in the analysis. A trapezoidal approximation rule was used which provided a close estimation to the analytical expressions and the simulation results. These results allow for low complexity analysis in XQAM fading channel systems where the channel behaviour is not independent.

6 Appendix

In a Nakagami-n fading channel the received signal from ith path is given by

$$y_i = \sqrt{E_s} h_i x + n_i \qquad i = 1,2 \tag{A.34}$$

where $h_i = (h_i^I + jh_i^Q) + (h_D^{I_i} + jh_D^{Q_i})$. The transformation matrix $\boldsymbol{T}$ is given by [25]

$$\boldsymbol{T} = \begin{bmatrix} \frac{\sqrt{2}}{2} & \frac{\sqrt{2}}{2} \\ -\frac{\sqrt{2}}{2} & \frac{\sqrt{2}}{2} \end{bmatrix} \tag{A.35}$$

Then we define another two random variables as

$$\begin{bmatrix} y_3 \\ y_4 \end{bmatrix} = \boldsymbol{T} \begin{bmatrix} y_1 \\ y_2 \end{bmatrix} = \begin{bmatrix} \frac{\sqrt{2}}{2} y_1 + \frac{\sqrt{2}}{2} y_2 \\ -\frac{\sqrt{2}}{2} y_1 + \frac{\sqrt{2}}{2} y_2 \end{bmatrix} \tag{A.36}$$

Based on (A.36) y_3 and y_4 are expressed as

$$y_3 = \left(h_3^I + jh_3^Q\right)x + n_3 \tag{A.37}$$

$$y_4 = \left(h_4^I + jh_4^Q\right)x + n_4 \tag{A.38}$$

where

$$h_3^I = \sqrt{E_s}\left[\left(\frac{\sqrt{2}}{2} h_1^I + \frac{\sqrt{2}}{2} h_2^I\right) + \frac{\sqrt{2}}{2}\left(h_D^{I_1} + h_D^{I_2}\right)\right] \tag{A.39.1}$$

$$h_3^Q = \sqrt{E_s}\left[\left(\frac{\sqrt{2}}{2} h_1^Q + \frac{\sqrt{2}}{2} h_2^Q\right) + \frac{\sqrt{2}}{2}\left(h_D^{Q_1} + h_D^{Q_2}\right)\right] \tag{A.39.2}$$

$$h_4^I = \sqrt{E_s}\left[\left(-\frac{\sqrt{2}}{2} h_1^I + \frac{\sqrt{2}}{2} h_2^I\right) + \frac{\sqrt{2}}{2}\left(-h_D^{I_1} + h_D^{I_2}\right)\right] \tag{A.39.3}$$

$$h_4^Q = \sqrt{E_s}\left[\left(-\frac{\sqrt{2}}{2} h_1^Q + \frac{\sqrt{2}}{2} h_2^Q\right) + \frac{\sqrt{2}}{2}\left(-h_D^{Q_1} + h_D^{Q_2}\right)\right] \tag{A.39.4}$$

$$n_3 = \frac{\sqrt{2}}{2} n_1 + \frac{\sqrt{2}}{2} n_2 \tag{A.39.5}$$

$$n_4 = -\frac{\sqrt{2}}{2} n_1 + \frac{\sqrt{2}}{2} n_2 \tag{A.39.6}$$

Since $E[h_1^I] = E[h_2^I] = 0$ and $E[(h_1^I)^2] = E[(h_2^I)^2] = \sigma^2$ the covariance of h_3^I and h_4^I can be calculated by

$$C_{h_3^I h_4^I} = E[h_3^I h_4^I] = 0 \tag{A.40}$$

The result of (40) indicates that h_3^I and h_4^I are uncorrelated and statistically independent. Similarly, we can also prove that h_3^Q and h_4^Q are also uncorrelated and statistically independent. Since $E\left[h_i^I h_j^Q\right] = 0, i = 1,2;\ j = 1,2$ we further can prove $E\left[h_i^I h_j^Q\right] = 0, i = 3,4;\ j = 3,4$. $E\left[h_i^I h_j^Q\right] = 0, i = 3,4;\ j = 3,4$, indicates that channel h_3 and h_4 are statistically independent.

So, the above transformation converts dual correlated Nakagami-n fading channel h_1 and h_2 into two independent fading channels, h_3 and h_4.

Without loss of generality we further assume $h_D^{I_2} = \beta h_D^{I_1}$ and $h_D^{Q_2} = \beta h_D^{Q_1}$. Then the mean values of h_3^I, h_3^Q, h_4^I and h_4^Q are derived as

$$E[h_3^I] = \frac{\sqrt{2}}{2}(1+\beta)h_D^{I_1} \tag{A.41.1}$$

$$E\left[h_3^Q\right] = \frac{\sqrt{2}}{2}(1+\beta)h_D^{Q_1} \tag{A.41.2}$$

$$E[h_4^I] = \frac{\sqrt{2}}{2}(\beta-1)h_D^{I_1} \tag{A.41.3}$$

$$E\left[h_4^Q\right] = \frac{\sqrt{2}}{2}(\beta-1)h_D^{Q_1} \tag{A.41.4}$$

The variances of h_3^I, h_3^Q, h_4^I, and h_4^Q are also derived as

$$E[(h_3^I)^2] = E_s(1+\rho)\sigma^2 + 0.5(1+\beta)^2 E_s\left(h_D^{I_1}\right)^2 \tag{A.42.1}$$

$$E\left[\left(h_3^Q\right)^2\right] = E_s(1+\rho)\sigma^2 + 0.5(1+\beta)^2 E_s\left(h_D^{Q_1}\right)^2 \tag{A.42.2}$$

$$E[(h_4^I)^2] = E_s(1-\rho)\sigma^2 + 0.5(1-\beta)^2 E_s\left(h_D^{I_1}\right)^2 \tag{A.42.3}$$

$$E\left[\left(h_4^Q\right)^2\right] = E_s(1-\rho)\sigma^2 + 0.5(1-\beta)^2 E_s\left(h_D^{Q_1}\right)^2 \tag{A.42.4}$$

In general, the results of (A.41a) to (A.42d) indicate that the transformation proposed in [25] converts dual correlated Nakagami-n fading channel $h_1$and h_2 with parameter K_1 and K_2 into two independent Nakagami-n fading channel h_3 and h_4 with K_3 and K_4 which are given by

$$K_3 = \frac{(1+\beta)^2}{4(1+\rho)\sigma^2}\left[\left(h_D^{I_1}\right)^2 + \left(h_D^{Q_1}\right)^2\right] \tag{A.43a}$$

$$K_4 = \frac{(1-\beta)^2}{4(1-\rho)\sigma^2}\left[\left(h_D^{I_1}\right)^2 + \left(h_D^{Q_1}\right)^2\right] \tag{A.43b}$$

Typically, when $h_D^{I_1} = h_D^{I_2}$ and $h_D^{Q_1} = h_D^{Q_2}$ $(\beta = 1)$ the transformation converts dual correlated Nakagami-n fading channels with equal parameter $K_1 = K_2$ into two independent fading channels, one is Rayleigh fading channel $(K_4 = 0)$, another still is Nakagami-n with parameter K_3 which is given by

$$K_3 = \frac{\left(h_D^{I_1}\right)^2 + \left(h_D^{Q_1}\right)^2}{(1+\rho)\sigma^2} \tag{A.44}$$

7 References

[1] J. Smith, "Odd-bit quadrature amplitude-shift keying," *IEEE Trans. on Commun.,* vol. 23, no. 3, pp. 385-389, 1975.

[2] S. Panigrahi and T. Le-Ngoc, "Fine-granularity loading schemes using adaptive Reed-Solomon coding for discrete multitone modulation systems," in *IEEE Int. Conf. on Commun.*, 2005.

[3] A. Ahrens and C. Lange, "Bit and power loading for wireline multicarrier transmission Systems," *Transactions on Advanced Research,* vol. 2(1), pp. 3-9, 2006.

[4] M. Zwingelstein-Colin, M. Gazalet and M. Gharbi, "Non-iterative bit-loading algorithm for ADSL-type DMT applications," *IEE Proc. Commun.,* vol. 150, no. 6, pp. 414–418, 2003.

[5] M. Sternad and S. Falahati, "Maximizing throughput with adaptive MQAM based on imperfect channel predictions," in *IEEE PIMRC*, Barcelona, 2004.

[6] W. Wang, T. Ottosson, M. Sternad, A. Ahlen and A. Svensson, "Impact of multiuser diversity and channel variability on adaptive OFDM," in *IEEE Vehic. Technol. Conf.*, Orlando, FL, 2004.

[7] "ITU-T Std. G.992.1, Asymmetric digital subscriber line (ADSL) transceivers," 1999.

[8] "ITU-T Std. G.993.1, Very high speed digital subscriber line transceivers," 2004.

[9] "ETSI Std. EN 300 429, Digital Video Broadcasting (DVB); Framing Structure, Channel Coding and Modulation for Cable Systems," 1998.

[10] M. Simon and M.-S. Alouini, Digital Communication over Fading Channels, Wiley-Interscience (New York), 2005.

[11] M. Nakagami, "The m-distribution—a general formula of intensity distribution of rapid fading," in *Statistical Methods in Radio Wave Propagation*, Pergamon, Oxford, Hoffman, W.G. (ed.), 1960.

[12] J. Salz and J. Winters, "Effect of fading correlation on adaptive arrays in digital mobile radio," *IEEE Trans. on Vehic. Technol.,* vol. 43, no. 4, pp. 1049–1057, Nov. 1994.

[13] V. Aalo, "Performance of maximal-ratio diversity systems in a correlated Nakagami fading environment," *IEEE Trans. on Commun.,* vol. 43, no. 8, pp. 2360-2369, Aug. 1995.

[14] A. Abu-Dayya and N. Beaulieu, "Switched diversity on microcellular Ricean channels," *IEEE Trans. on Vehic. Technol.,* vol. 43, no. 4, pp. 970-976, 1994.

[15] E. Al-Hussaini and A. Al-Bassiouni, "Performance of MRC diversity systems for the detection of signals with Nakagami fading," *IEEE Trans. on Commun.,* vol. 33, no. 12, pp. 1315-1319, 1985.

[16] Bithas P.S and P. Mathiopoulos , "Performance analysis of SSC diversity receivers over correlated Ricean fading satellite channels," *EURASIP J. Wirel. Commun. Netw.,* May 2007.

[17] X.-C. Zhang, H. Yu and G. Wei, "Exact Symbol error probability of cross-QAM in AWGN and fading channels," *EURASIP J. Wirel. Commun. Netw.,* pp. 1–9, 2010.

[18] H. Yu, Y. Zhao, J. Zhang and Y. Wang, "SEP Performance of Cross QAM Signaling with MRC over Fading Channels and its Arbitrarily Tight Approximation," *Wireless Pers. Commun.,* vol. 69, no. 4, pp. 1567-1582, 2013.

[19] H. Yu, G. Wei, F. Ji and X. Zhang, "On the error probability of cross-QAM with MRC reception over generalized η-μ fading channels," *IEEE Trans. on Vehic. Technol.,* vol. 60, no. 6, pp. 2631-2643, 2011.

[20] M. Chiani, D. Dardari and M. K. Simon, "New exponential bounds and approximations for the computation of error probability in fading channels," *IEEE Trans. on Wireless Commun.,* vol. 2, no. 7, pp. 840-845, Jul. 2003.

[21] H. Xu, "Symbol error probability for generalized selection combining reception of M-QAM," *SAIEE Africa Res. Journ.,* vol. 100, no. 3, pp. 68-71, Sep. 2009.

[22] S. Jovkovic, S. Panic, M. Stefanovic, P. Spalevic and D. Krstic, "Performance Analysis of SSC Diversity Receiver over Correlated Ricean Fading Channels in the Presence of Cochannel Interference," *EURASIP J. Wirel. Commun. Netw.,* 2010.

[23] G. Karagiannidis, "Performance Analysis of SIR-Based Dual Selection Diversity over Correlated Nakagami-m Fading Channels," *IEEE Trans. on Vehic. Technol.,* vol. 52, no. 5, pp. 1207-1216, Sep. 2003.

[24] V. Veeravalli, "On Performance Analysis for Signaling on Correlated Fading Channels," *IEEE Trans. Commun.,* vol. 49, no. 11, p. 1879–1883, Nov. 2001.

[25] L. Fang, G. Bi and A. Kot, "New Method of Performance Analysis for Diversity Reception with Correlated Rayleigh-fading Signals," *IEEE Trans. on Vehic. Technol.,* vol. 49, no. 5, pp. 1807-1812, Sep. 2000.

PAPER B

In preparation for submission

Performance Analysis of Cross QAM with MRC over Non-Identical Correlated Fading Channels

Muhammad Wazeer Kamdar and Hongjun Xu

Abstract

An approximation expression is derived for the symbol error probability (SEP) of a single-input multiple-output (SIMO) cross QAM (XQAM) modulated system over an arbitrary number of non-identical, correlated fading channels. Rayleigh, Nakagami-m and Nakagami-q fading channels are considered. SEP expressions for independent channels are derived using the MGFs for the fading channels, with MRC diversity combining. A transformation technique is proposed that uses knowledge of the channel covariance matrix to convert an arbitrary number of non-identical, correlated fading channels into identically distributed, independent channels. Simulations are performed in Matlab to verify the accuracy of the derived expressions.

1 Introduction

Quadrature amplitude modulation (QAM) is a popular method for modulating signals in digital communication systems as it achieves high bandwidth and power efficiency. The square QAM is used for systems with even bit constellations while cross QAM (XQAM) and rectangular QAM are used for systems with odd bit constellations. It was shown in [1] that XQAM achieves better error performance than rectangular QAM. XQAM is already used in adaptive modulation schemes [2-6], blind equalization [7] as well as various practical systems [8-10].

Error performance analysis of XQAM for various fading channel conditions has been discussed in the literature. In [11], closed-form expressions were derived for the symbol error probability (SEP) of XQAM over the additive white Gaussian noise (AWGN) and independent fading channels. In [12], approximate closed-form expressions for the SEP of XQAM with MRC over independent Nakagami-m, -n and -q fading channels were derived. In [13], SEP expressions for independent generalized $\eta - \mu$ fading channels were derived. In [14], expressions for the SEP of XQAM over dual correlated Nakagami fading channels were derived.

Error performance analysis for systems employing XQAM has also been discussed in the literature. In [15], an exhaustive Gaussian approach (EGA) is proposed for BER performance analysis of direct-detection orthogonal frequency division multiplexing (DD-OFDM) systems, where both square QAM and XQAM are considered as the modulation scheme. In [16], error performance analysis for XQAM in free space optical (FSO) systems under the effect of generalized pointing errors and atmospheric turbulence was investigated.

In the literature, various methods have been proposed in order to analyse SEP performance for systems with correlated fading channels [17-19]. The transformation technique in [20] was used in [14], which produces dual independent fading channels from a pair of dual correlated fading channels. The equivalent system with independent channels could then be analysed using known expressions for the SEP of XQAM.

From the above literature survey, [12] considered an arbitrary number of non-identical, independent fading channels, and [14] only considered dual correlated, identical fading channels. However, a system comprised of an arbitrary number of channels that are both non-identical and correlated has not been discussed. In this paper, we expand upon the work done in [11-14] to consider the transmission of XQAM over an arbitrary number of correlated, non-

identical Rayleigh, Nakagami-m, and Nakagami-q channels. The transformation technique in [20] is an order two orthogonal transformation matrix. However, there does not exist an orthogonal transformation matrix for arbitrary order which is greater than or equal to three. Therefore, this transformation technique in [20] cannot be extended to systems comprising more than two channels. However, the transformation technique used in [20] motivates us to apply the singular value decomposition (SVD) factorization approach in this paper. By performing SVD on the channel covariance matrix, we can perform a linear transformation on a set of correlated, non-identical channels of arbitrary order.

In order to derive the error performance of the system, approximations for the Q-function and generalized Q-function are firstly obtained using the trapezoidal rule, as was done in [14]. Secondly, the moment generating function (MGF) is used to obtain expressions for the SEP over an arbitrary number of non-identical fading channels. Lastly, knowledge of the correlation matrix of the above system is used to transform a system with correlated channels of arbitrary order into equivalent independent channels.

The remainder of this paper is organized as follows. In section 2, the system model and system parameters are detailed. In Section 3, expressions are derived for the SEP of XQAM over multiple non-identical correlated fading channels. In Section 4, simulated and analytical results are presented. Section 5 concludes the discussion.

2 System model

Consider a single-input multiple-output (SIMO) system ($N_R \times 1$), where N_R ($N_R \geq 2$) denotes the number of receive antennas. The system employs M-ary XQAM modulation, with $M = 32, 128$ and 512 being considered in this paper. The fading channels from N_R receive antennas are considered as correlated and non-identical. The fading channels are modelled using Rayleigh, Nakagami-m or Nakagami-q fading channel distributions. The received signal can be written as

$$\boldsymbol{y} = \sqrt{E_s}\boldsymbol{H}x + \boldsymbol{n} \tag{B. 1}$$

where $\boldsymbol{y} = [y_1\ y_2 \cdots\ y_{N_R}]^T$ is the received signal vector, x is the transmitted XQAM symbol with $E[|x|^2] = 1$, E_s is the transmit symbol power, $\boldsymbol{n} = [n_1\ n_2 \cdots n_{N_R}]^T$ is the complex additive white Gaussian noise (AWGN) vector, and $\boldsymbol{H} = \left[h_1\ h_2 \cdots h_{N_R}\right]^T$ is the fading channel vector with amplitudes $\boldsymbol{\alpha} = \left[\alpha_1\ \alpha_2 \cdots \alpha_{N_R}\right]^T$ and $h_i = h_i^I + jh_i^Q,\ i \in [1{:}\,N_R]$ where h_i^I and h_i^Q are real Gaussian random variables. The entries of $n_i,\ i \in [1{:}\,N_R]$ and $h_i,\ i \in [1{:}\,N_R]$ comprise independent and identically distributed (IID) entries according to the complex Gaussian distribution with $CN(0,1)$ and $CN(0,\sigma_{h_i}^2)$ respectively.

It is assumed that

$$E\left[h_i^I\right] = E\left[h_i^Q\right] = 0, \qquad i \in [1{:}\,N_r] \tag{B. 2.1}$$

$$E\left[\left(h_i^I\right)^2\right] = \left(\sigma_i^I\right)^2, \qquad i \in [1{:}\,N_r] \tag{B. 2.2}$$

$$E\left[\left(h_i^Q\right)^2\right] = \left(\sigma_i^Q\right)^2, \qquad i \in [1{:}\,N_r] \tag{B. 2.3}$$

$$E[h_i] = 0, \qquad i \in [1{:}\,N_r] \tag{B. 2.4}$$

$$E\left[h_j^I h_k^Q\right] = 0, \qquad j,k \in [1{:}\,N_r] \tag{B. 2.5}$$

$$C_{h_j h_k} = E\left[h_j h_k^*\right] = \rho_{jk}\sigma_{h_j}\sigma_{h_k}, \qquad j,k \in [1{:}\,N_r] \tag{B. 2.6}$$

$$E[n_i n_k^*] = E\left[n_j h_k^*\right] = 0, \qquad i,j,k \in [1{:}\,N_r];\ i \neq k \tag{B. 2.7}$$

where ρ_{jk} is the correlation coefficient between channels h_j and h_k, and $\sigma_{h_i} = \sqrt{\left(\sigma_i^I\right)^2 + \left(\sigma_i^Q\right)^2}$ is the standard deviation of channel h_i. For Rayleigh and Nakagami-m channels, $\sigma_i^I = \sigma_i^Q$ whilst for Nakagami-Q, $\sigma_i^I = q\sigma_i^Q$, where q is the Hoyt parameter. It is also assumed that there exist at least two channels $h_i, i \in [1{:}\,N_r]$ and $h_k, k \in [1{:}\,N_r],\ i \neq k$, that

are non-identical i.e. $E[|h_i|^2] \neq E[|h_k|^2]$. Note that for the special case of identically distributed channels, it is assumed that $E[|h_i|^2] = 1,\ \ i = 1, \cdots, N_R$ and the covariance between channels is dependent only on the correlation between them i.e. $C_{h_j h_k} = \rho_{jk},\ \ j, k \in [1: \mathrm{N}_R]$.

3 SEP of XQAM over Non-identical, Correlated Fading Channels

As discussed in the introduction, knowledge of the covariance matrix is used to convert a system of correlated, non-identical channels of arbitrary order into independent channels. However, we first need to derive error performance analysis for a set of independent channels. We begin by considering error performance analysis of a single fading channel (Section 3.1). Using MRC and the MGF approach, we can extend the analysis to a multichannel, uncorrelated system (Section 3.2). Finally, we need to convert a set of correlated, non-identical channels into a set of independent channels in order to apply the results from Section 3.2. Therefore, in Section 3.3, we apply the proposed transformation technique to the system of correlated, non-identical channels, and derive all system parameters for the resulting equivalent system.

3.1 SEP of XQAM over a single fading channel

The exact SEP of XQAM over AWGN, P_{exa} has been derived in [11, eq. 22]. Since this equation contains the Gaussian Q-function, a tight approximate expression, P_s, is derived in [14, eq. 20] that uses the trapezoidal rule to approximate the Gaussian Q-function, resulting in a closed-form expression.

The average SEP of XQAM over a single fading channel is then derived by averaging the approximated SEP expression over the fading distribution of the instantaneous received SNR, γ, as given by [14, eq. 21] as $P_s(\bar{\gamma}) = \int_0^\infty P_s(\gamma) p_\gamma(\gamma)\, d\gamma$. Depending on the fading channel model under consideration, we can replace $p_\gamma(\gamma)$ by $p_{\gamma_R}(\gamma)$ for Rayleigh, $p_{\gamma_m}(\gamma)$ for Nakagami-m, or $p_{\gamma_q}(\gamma)$ for Nakagami-q, as defined in [14, eq. 3-5].

Using the MGF function $M_\gamma(s) = \int_0^\infty \exp(-s\gamma) p_\gamma(\gamma) d\gamma$, we can alternatively express $P_s(\bar{\gamma})$ as [14. eq.22]:

$$P_s(\bar{\gamma}) = \frac{g_1}{8m} \cdot M_\gamma(-A_o) - \frac{g_2}{8m} \cdot M_\gamma(-2A_o) + \frac{g_1}{4m} \cdot \sum_{p=1}^{m-1} M_\gamma\left(\frac{-A_o}{\sin^2(\vartheta_p)}\right)$$

$$- \frac{g_2}{4m} \cdot \sum_{p=1}^{m-1} M_\gamma\left(\frac{-A_o}{\sin^2(\vartheta_p)}\right) + \frac{1}{2mM} \cdot M_\gamma(-A_1) + \frac{1}{mM} \cdot \sum_{p=1}^{2m-1} M_\gamma\left(\frac{-A_1}{\sin^2(\vartheta_p)}\right)$$

$$+ \frac{4}{M\pi n} \cdot \sum_{k=1}^{v-1} \alpha_k \cdot M_\gamma\left(\frac{-A_o}{\sin^2(\alpha_k)}\right) + \frac{8}{M\pi n} \cdot \sum_{k=1}^{v-1} \alpha_k \cdot \left(\sum_{p=1}^{n-1} M_\gamma\left(\frac{-A_o}{\sin^2\left(\frac{p\alpha_k}{n}\right)}\right)\right)$$

$$+ \frac{4}{M\pi n} \cdot \sum_{k=1}^{v-1} \beta_k^- \left[\frac{1}{2} \cdot M_\gamma\left(\frac{-A_o}{\sin^2(\beta_k^-)}\right) + \sum_{p=1}^{n-1} M_\gamma\left(\frac{-A_o}{\sin^2\left(\frac{p\beta_k^-}{n}\right)}\right)\right]$$

$$-\frac{4}{M\pi n}\cdot\sum_{k=1}^{v-1}\beta_k^+\left[\frac{1}{2}\cdot M_\gamma\left(\frac{-A_o}{\sin^2(\beta_k^+)}\right)+\sum_{p=1}^{n-1}M_\gamma\left(\frac{-A_o}{\sin^2\left(\frac{p\beta_k^+}{n}\right)}\right)\right] \tag{B.3}$$

where n is the number of summations which is convergent for $n > 10,$ and

$$g_1 = 4-\frac{6}{\sqrt{2M}} \tag{B.3.1}$$

$$g_2 = 4-\frac{12}{\sqrt{2M}}+\frac{12}{M} \tag{B.3.2}$$

$$v = \frac{1}{8}\sqrt{2M} \tag{B.3.3}$$

$$A_0 = \frac{48}{31M-32} \tag{B.3.4}$$

$$A_k = 2k^2A_0, \qquad k\in[1:v] \tag{B.3.5}$$

$$\alpha_k = \arctan\left(\frac{1}{2k+1}\right), \qquad k\in[1:v-1] \tag{B.3.6}$$

$$\beta_k^- = \arctan\left(\frac{k}{k-1}\right), \qquad k\in[2:v] \tag{B.3.7}$$

$$\beta_k^+ = \arctan\left(\frac{k}{k+1}\right), \qquad k\in[1:v-1] \tag{B.3.8}$$

$$m = 2n \tag{B.3.9}$$

$$\vartheta_p = \frac{p\pi}{4m} \tag{B.3.10}$$

Depending on the fading channel model under consideration, we can replace $M_\gamma(s)$ in (B.3) by $M_{\gamma_R}(s)$ for Rayleigh, $M_{\gamma_m}(s)$ for Nakagami-m or $M_{\gamma_q}(s)$ for Nakagami-q, as defined in [14, eq. 7-9]. A full derivation for (B.3) can be found in [14].

3.2 MRC diversity reception for multiple independent fading channels

Given a system of N_R non-identical, independent channels with MRC diversity reception, the PDF of the instantaneous SNR at the receiver is given by

$$p_\gamma(\gamma) = \prod_{i=1}^{N_R} p_{\gamma_i}(\gamma_i) \tag{B.4}$$

where γ_i is the instantaneous SNR for path $i,\ i\in[1:N_R]$

Then the MGF of γ becomes

$$M_\gamma(s) = E\{e^{-s\gamma}\} = E\left\{e^{-s(\gamma_1+\gamma_2+\cdots+\gamma_{N_R})}\right\} = \prod_{i=1}^{N_R} M_{\gamma_i}(s) \tag{B.5}$$

For the case of identically distributed channels, (B.5) simplifies to

$$M_{\gamma}(s) = \left(M_{\gamma_1}(s)\right)^{N_R} \tag{B.6}$$

For a system of N_R identical, independent channels, we can use the results from (B.6) in place of $M_{\gamma}(s)$ in (B.3).

3.3 Approximated SEP of XQAM over non-identical, correlated fading channels

In order to analyse the SEP of XQAM over non-identically distributed, correlated fading channels, the following method can be used assuming the covariance between each pair of correlated fading channels is known.

Given a set of N_R uncorrelated, identically distributed, zero-mean and unit variance complex Gaussian random variables $\boldsymbol{H}_u = \left[h_{u_1}\, h_{u_2} \cdots\, h_{u_{N_R}}\right]^T$, we can obtain a set of correlated, non-identical, zero-mean complex Gaussian random variables $\boldsymbol{H}_c = \left[h_{c_1}\, h_{c_2} \cdots\, h_{c_{N_R}}\right]^T$ by applying a linear transformation to $\boldsymbol{H}_u$:

$$\boldsymbol{H}_c = \boldsymbol{A}\boldsymbol{H}_u \tag{B.7}$$

where $\boldsymbol{A} = \begin{bmatrix} A_{1,1} & \cdots & A_{1,N_R} \\ \vdots & \ddots & \vdots \\ A_{N_R,1} & \cdots & A_{N_R,N_R} \end{bmatrix}$.

The $N_R \times N_R$ covariance matrix of $\boldsymbol{H}_c$ is given by

$$\boldsymbol{C}_{H_C} = E\left[\boldsymbol{H}_c {\boldsymbol{H}_c}^H\right] = E[(\boldsymbol{A}\boldsymbol{H}_u)(\boldsymbol{A}\boldsymbol{H}_u)^H] = \boldsymbol{A}E\left[\boldsymbol{H}_u {\boldsymbol{H}_u}^H\right]\boldsymbol{A}^H = \boldsymbol{A}\boldsymbol{C}_{\boldsymbol{H}_u}\boldsymbol{A}^H = \boldsymbol{A}\boldsymbol{A}^H \tag{B.8}$$

where $\boldsymbol{C}_{\boldsymbol{H}_u}$ is the covariance matrix of $\boldsymbol{H}_u$, which is the $N_R \times N_R$ identity matrix since the channels of $\boldsymbol{H}_u$ are uncorrelated and have unit variance.

The covariance matrix $\boldsymbol{C}_{H_C}$ can also be expressed as

$$\boldsymbol{C}_{H_C} = \begin{bmatrix} C_{1,1} & \cdots & C_{1,N_R} \\ \vdots & \ddots & \vdots \\ C_{N_R,1} & \cdots & C_{N_R,N_R} \end{bmatrix} \tag{B.9}$$

where the entries $C_{jk} = \rho_{jk}\sigma_j\sigma_k$, $j \in [1{:}\,N_R]$ $k \in [1{:}\,N_R]$. For the special case of identically distributed channels, $C_{jk} = \rho_{jk}$ and the entries in the main diagonal are equal to 1. Since $\boldsymbol{C}_{H_C}$ is a symmetric square matrix, we can perform a singular value decomposition (SVD) on $\boldsymbol{C}_{H_C}$:

$$\boldsymbol{C}_{H_C} = \boldsymbol{V}\boldsymbol{D}\boldsymbol{V}^H \tag{B.10}$$

where $\boldsymbol{V}$ is an $N_R \times N_R$ orthogonal matrix with columns equal to the eigenvectors of $\boldsymbol{C}_{H_C}\boldsymbol{C}_{H_c}^H$, and $\boldsymbol{D}$ is a diagonal matrix whose diagonal entries are the eigenvalues of $\boldsymbol{C}_{H_C}$.

Define $\boldsymbol{A} = \boldsymbol{V}\sqrt{\boldsymbol{D}}$. From this it follows:

$$\boldsymbol{A}\boldsymbol{A}^H = \left(\boldsymbol{V}\sqrt{\boldsymbol{D}}\right)\left(\boldsymbol{V}\sqrt{\boldsymbol{D}}\right)^H = \boldsymbol{V}\boldsymbol{D}\boldsymbol{V}^H = \boldsymbol{C}_{H_C} \tag{B.11}$$

Since this is a linear transformation, the process can be reversed. Therefore, given a set of non-identical, correlated random variables $\boldsymbol{H}_c$, we can apply a linear transform $\boldsymbol{B}$ to obtain a set of uncorrelated, identically distributed random variables $\boldsymbol{H}_u$:

$$\boldsymbol{H}_u = \boldsymbol{B}\boldsymbol{H}_c \tag{B.12}$$

where $\boldsymbol{B} = \boldsymbol{A}^{-1}$, where $\boldsymbol{A}^{-1}$ is the inverse matrix of $\boldsymbol{A}$. A derivation for the average SNR of the equivalent independent fading channels is shown below:

Let $\boldsymbol{B} = \begin{bmatrix} b_{1,1} & \cdots & b_{1,N_R} \\ \vdots & \ddots & \vdots \\ b_{N_R,1} & \cdots & b_{N_R,N_R} \end{bmatrix}$

Replacing $\boldsymbol{H}$ by $\boldsymbol{H}_c$ in (B.1), the received signal is given by

$$\boldsymbol{y} = \sqrt{E_s}\boldsymbol{H}_c x + \boldsymbol{n} \tag{B.13}$$

Multiplying by $\boldsymbol{B}$:

$$\boldsymbol{B}\boldsymbol{y} = \sqrt{E_s}\boldsymbol{B}\boldsymbol{H}_c x + \boldsymbol{B}\boldsymbol{n} \tag{B.14}$$

Define $\tilde{\boldsymbol{y}} = \boldsymbol{B}\boldsymbol{y}$ where $\tilde{\boldsymbol{y}} = \left[\tilde{y}_1\ \tilde{y}_2 \cdots\ \tilde{y}_{N_R}\right]^T$ and $\tilde{y}_i = b_{i1}y_1 + \cdots + b_{iN_R}y_{N_R}$. Define $\tilde{\boldsymbol{n}} = \boldsymbol{B}\boldsymbol{n}$ where $\tilde{\boldsymbol{n}} = \left[\tilde{n}_1\ n_2 \cdots\ \tilde{n}_{N_R}\right]^T$ and $\tilde{n}_i = b_{i1}n_1 + \cdots + b_{iN_R}n_{N_R}$, where $\tilde{n}_i$ is zero-mean and variance is $|b_{i1}|^2 + \cdots + \left|b_{iN_R}\right|^2$. We can then write (B.14) as

$$\tilde{\boldsymbol{y}} = \sqrt{E_s}\boldsymbol{H}_u x + \tilde{\boldsymbol{n}} \tag{B.15}$$

For each equivalent received signal i the average SNR $\bar{\gamma}_i$ is

$$\bar{\gamma}_i = \frac{1}{b_{i1}^2 + \cdots + b_{iN_R}^2}\bar{\gamma}, \qquad i \in [1{:}\ N_R] \tag{B.16}$$

Since the channels of the equivalent system are identically distributed and independent, we can express the MGF of γ using (B.16) and (B.6) in (B.3).

4 Simulation Results

The computer simulations in this section were done using the Monte Carlo method and a sample size of 10^7. For this set of simulations, each system consisted of three channels (three receivers). Simulations were performed for Rayleigh, Nakagami-m, and Nakagami-q (Hoyt) fading channels. For the simulation results, symbol detection was performed using the actual received signals from (B.1), whilst for the theoretical results, symbol detection used the equivalent received signals from (B.16). Two sets of simulations were performed: one with non-identical channels, and one with identically distributed channels.

Simulations were performed with the following system parameters for Fig. B1 to Fig. B3: Variance for the correlated channels $\sigma_{h_1}^2 = 1$, $\sigma_{h_2}^2 = 0.8$ and $\sigma_{h_3}^2 = 0.5$ for non-identical channels, and $\sigma_{h_i}^2 = 1$, $i = 1,2,3$ for identical channels. Correlation coefficients $\rho_{12} = 0.3$, $\rho_{13} = 0.4$, and $\rho_{23} = 0.6$. Nakagami-m coefficient $m = 3$ and Hoyt parameter $q = 0.6$. Constellation sizes of $M = 32, 128$ and 512 were considered. Simulation results are shown in Fig. B.1 to Fig. B.3 for Rayleigh, Nakagami-m, and Nakagami-q, respectively. Simulation results are presented together with the corresponding numerical result using the expressions derived in section 3. The figures show a good match between simulation and analytical results.

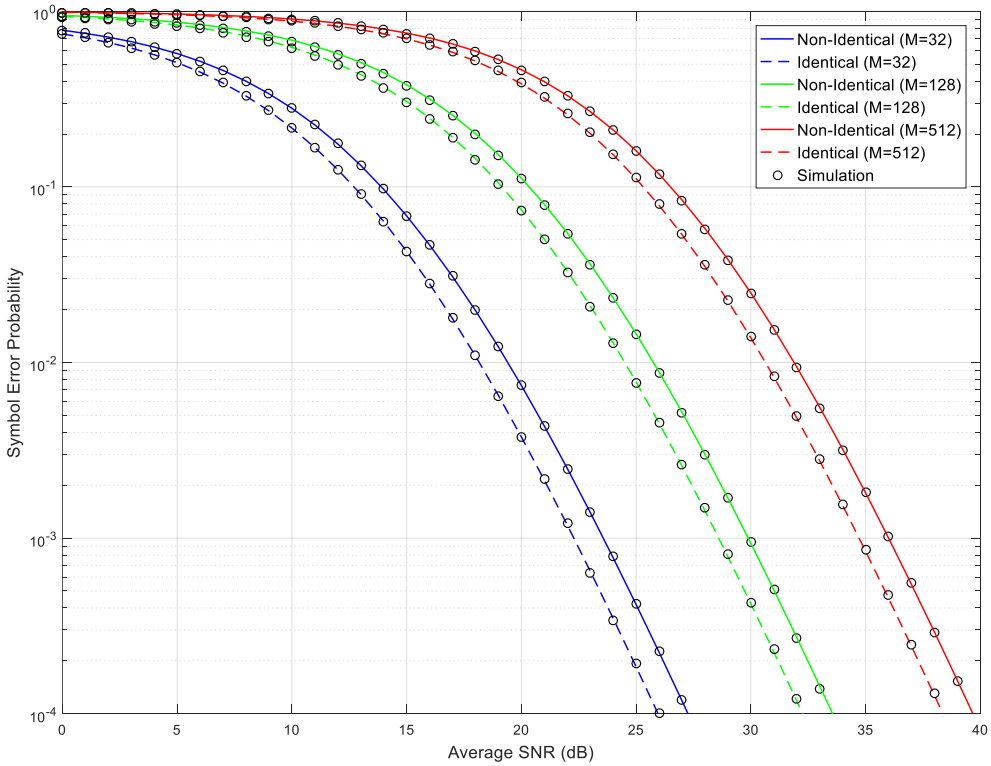

Fig. B.1 Rayleigh channels

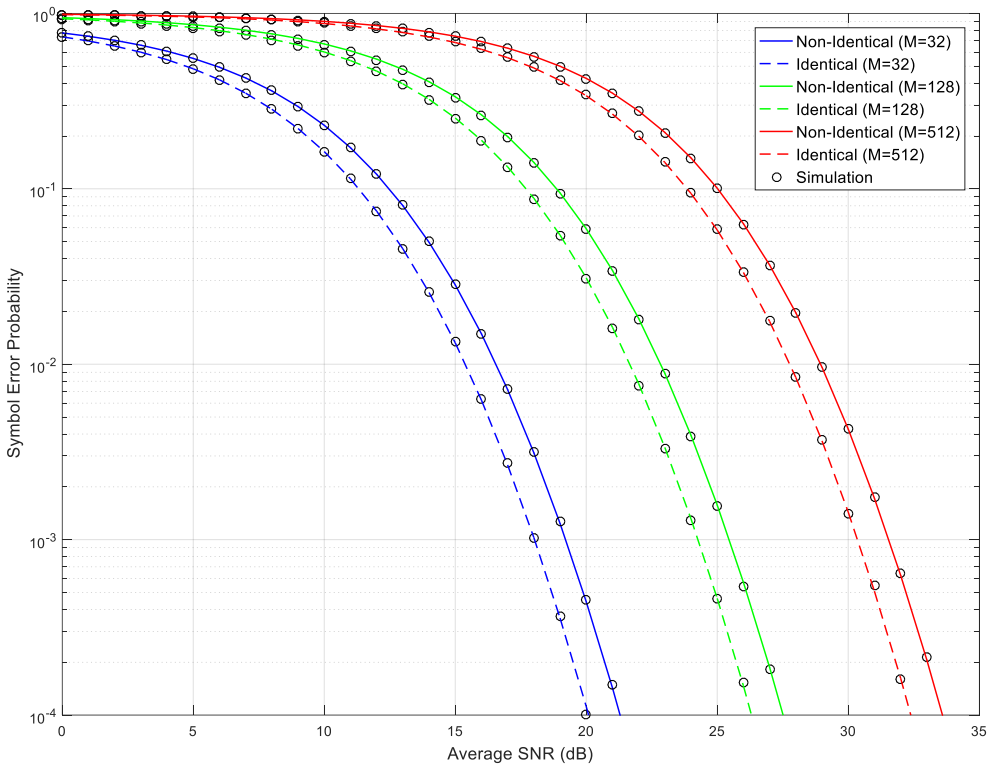

Fig. B.2 Nakagami-m channels

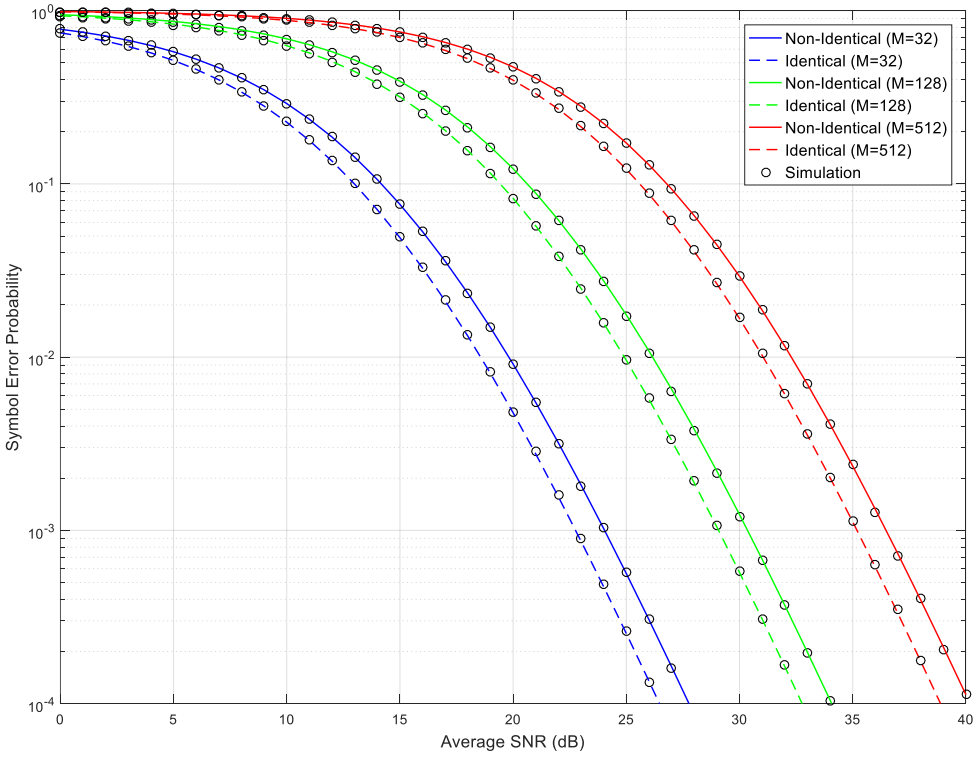

Fig. B.3 Nakagami-q channels

5 Conclusion

In this paper, expressions for the SEP of XQAM over non-identical correlated Rayleigh, Nakagami-m, and Nakagami-q fading channels using the MGF method have been derived. A transformation technique was presented that was then used to produce equivalent independent fading channels from an arbitrary number of non-identical, correlated fading channels. These results allow us to analyse XQAM systems of arbitrary order where the channels experience correlated behaviour and are non-identically distributed, provided knowledge of the channel covariance matrix is known. Further research will need to be conducted to provide a solution that does not require knowledge of the covariance matrix.

6 References

[1] J. Smith, "Odd-bit quadrature amplitude-shift keying," *IEEE Trans. on Commun.,* vol. 23, no. 3, pp. 385-389, 1975.

[2] S. Panigrahi and T. Le-Ngoc, "Fine-granularity loading schemes using adaptive Reed-Solomon coding for discrete multitone modulation systems," in *IEEE Int. Conf. on Commun.*, 2005.

[3] A. Ahrens and C. Lange, "Bit and power loading for wireline multicarrier transmission Systems," *Transactions on Advanced Research,* vol. 2(1), pp. 3-9, 2006.

[4] M. Zwingelstein-Colin, M. Gazalet and M. Gharbi, "Non-iterative bit-loading algorithm for ADSL-type DMT applications," *IEE Proc. Commun.,* vol. 150, no. 6, pp. 414–418, 2003.

[5] M. Sternad and S. Falahati, "Maximizing throughput with adaptive MQAM based on imperfect channel predictions," in *IEEE PIMRC*, Barcelona, 2004.

[6] W. Wang, T. Ottosson, M. Sternad, A. Ahlen and A. Svensson, "Impact of multiuser diversity and channel variability on adaptive OFDM," in *IEEE Vehic. Technol. Conf.*, Orlando, FL, 2004.

[7] S. Abrar and I. Qureshi, "Blind equalization of cross-QAM signals," *IEEE Sig. Proc. Lett.,* vol. 13, no. 12, pp. 745-748, 2006.

[8] "ITU-T Std. G.992.1, Asymmetric digital subscriber line (ADSL) transceivers," 1999.

[9] "ITU-T Std. G.993.1, Very high speed digital subscriber line transceivers," 2004.

[10] "ETSI Std. EN 300 429, Digital Video Broadcasting (DVB); Framing Structure, Channel Coding and Modulation for Cable Systems," 1998.

[11] X.-C. Zhang, H. Yu and G. Wei, "Exact Symbol error probability of cross-QAM in AWGN and fading channels," *EURASIP J. Wirel. Commun. Netw.,* pp. 1–9, 2010.

[12] H. Yu, Y. Zhao, J. Zhang and Y. Wang, "SEP Performance of Cross QAM Signaling with MRC over Fading Channels and its Arbitrarily Tight Approximation," *Wireless Pers. Commun.,* vol. 69, no. 4, pp. 1567-1582, 2013.

[13] H. Yu, G. Wei, F. Ji and X. Zhang, "On the error probability of cross-QAM with MRC reception over generalized η-μ fading channels," *IEEE Trans. on Vehic. Technol.,* vol. 60, no. 6, pp. 2631-2643, 2011.

[14] M. Kamdar and H. Xu, "SEP Performance Analysis of Cross QAM with MRC over Dual Correlated Nakagami-m, -n, and -q Channels," *Wireless Pers. Commun.,* vol. 84, no. 4, pp. 3015-3030, 2015.

[15] P. Cruz, J. Rosario, T. Alves and A. Cartaxo, "Exhaustive gaussian approach for performance evaluation of direct-detection OFDM systems employing square and cross QAM," in *2014 ITS*, Sao Paulo, Aug. 2014.

[16] N. Sharma and P. Garg, "Cross-QAM Signaling in Free Space Optical Communication Systems with Generalized Pointing Errors," in *IEEE VTC-Fall*, Toronto, Sep. 2017.

[17] S. Jovkovic, S. Panic, M. Stefanovic, P. Spalevic and D. Krstic, "Performance Analysis of SSC Diversity Receiver over Correlated Ricean Fading Channels in the Presence of Cochannel Interference," *EURASIP J. Wirel. Commun. Netw.,* 2010.

[18] G. Karagiannidis, "Performance Analysis of SIR-Based Dual Selection Diversity over Correlated Nakagami-m Fading Channels," *IEEE Trans. on Vehic. Technol.,* vol. 52, no. 5, pp. 1207-1216, Sep. 2003.

[19] V. Veeravalli, "On Performance Analysis for Signaling on Correlated Fading Channels," *IEEE Trans. on Commun.,* vol. 49, no. 11, p. 1879–1883, Nov. 2001.

[20] L. Fang, G. Bi and A. Kot, "New Method of Performance Analysis for Diversity Reception with Correlated Rayleigh-fading Signals," *IEEE Trans. on Vehic. Technol.,* vol. 49, no. 5, pp. 1807-1812, Sep. 2000.

[21] M. Simon and M.-S. Alouini, Digital Communication over Fading Channels, Wiley-Interscience (New York), 2005.

PAPER C

In preparation for submission

Uncoded Space-Time Labeling Diversity for Cross QAM with MPSK

Muhammad Wazeer Kamdar, Hongjun Xu and Narushan Pillay

Abstract

An uncoded space-time labeling diversity (USTLD) system with improved bandwidth efficiency for cross quadrature amplitude modulation (XQAM) is proposed. The proposed system is a combination of USTLD with XQAM and M-ary phase shift keying (MPSK) modulation. A low complexity (LC) detection scheme is proposed based on the maximum likelihood (ML) detection scheme. A simple approach is discussed to design mappers for XQAM and MPSK which are then used in the proposed system. Rayleigh flat-fading conditions are considered, and the tightness achieved by a theoretical average bit error probability (ABEP) bound is investigated. By introducing extra bits to a USTLD system via a 16PSK phase component, the data rate for 32XQAM and 128XQAM USTLD can be improved by 20% and 14.3% respectively. Simulation results show that the error performance of the proposed system with improved bandwidth efficiency closely matches performance of the standard USTLD system at high SNR.

1 Introduction

In order to improve the reliability of a communication system, various diversity techniques have been developed. One such technique that has found application in space-time coded systems is labeling diversity. By applying different labeling maps to the spatial streams at the transmitter, the system error performance can be improved.

In the literature, labeling diversity has found applications in both coded and uncoded systems. Labeling diversity was first used in coded systems. Bit-interleaved coded modulation with iterative decoding (BICM-ID), proposed in [1], is a scheme that produces a large coding gain at a lower system complexity than alternatives such as turbo trellis coded modulation (TCM). BICM-ID can also be combined with space-time diversity in multiple-input multiple-output (MIMO) systems [BI-STCM-ID]. In [2], it was shown that the choice of labeling map significantly affected system performance. In [3], optimal labeling criterion for BI-STCM-ID over Rayleigh-fading channels was documented. Other work in the literature that relates to the design of the mapper is presented in [4-6]. Other applications for labeling diversity include wireless relay networks and hybrid automatic repeat request (HARQ) [7-9].

Recently, the authors in [10] proposed uncoded space-time labeling diversity (USTLD), which combined an uncoded labeling diversity scheme with a space-time block code (STBC) system. USTLD was shown to have lower complexity and higher bandwidth efficiency than BI-STCM-ID. Mapper design criterion was proposed, as well as a simple method for generating a mapper. Based on the work in [10], various systems have been proposed in the literature. In [11], a USTLD system using three transmit antennas was proposed, resulting in an improved BER performance. In [12], space-time block coded spatial modulation with labeling diversity (STBC-SM-LD) was proposed, by applying labeling diversity to STBC-SM. In [13], signal space diversity (SSD) was applied to a USTLD system (SSD-USTLD), which showed improved performance over USTLD. In [14] the error performance of USTLD in spatially correlated Nakagami-q channels was investigated.

The systems in [11-14] considered only error performance of USTLD. One of the other key objectives in the design of communication systems is bandwidth or spectral efficiency. This is due to the limited available frequency spectrum for wireless communications. Various works in the literature are dedicated to improving the spectral efficiency of a STBC system. In [15], a scheme to improve spectral efficiency by improving Alamouti code efficiency is proposed,

though the scheme only shows meaningful results for two transmit antenna systems. In [16], high data rate Alamouti codes (HDRAC) was proposed that used field extensions, though ML detection for the scheme had high complexity. In [17], a high-rate STBC using QPSK for both 2 and 4 transmit antenna systems were proposed but did not achieve significant spectral efficiency improvement. In [18], a new space-time full-rate code called embedded Alamouti space-time (EAST) was proposed. In [19-20], additional schemes that combine spatial modulation with STBC are presented. However, the systems cannot achieve transmit diversity with only two transmit antennas. In [21], a trellis code-aided STLD system was proposed, which improved spectral efficiency by using trellis coding to map additional bits. However, as this is a coded scheme, it cannot be applied to USTLD.

The motivation of this paper is as follows. Firstly, as mentioned, the systems in [11-14] improve only upon the error performance of USTLD, not the spectral efficiency. Secondly, only square QAM constellations have been considered in the above systems. Square QAM is only applicable to even-bit constellations, not odd-bit. Further, the mapper design is not applicable to odd-bit constellations such as rectangular QAM or cross-quadrature amplitude modulation **(**XQAM). Lastly, the scheme proposed in [21] motivates the idea of achieving higher spectral efficiency by mapping additional bits. In order to achieve this for an uncoded system, we propose the following system in this paper. A USTLD system with XQAM is considered**.** XQAM is chosen over rectangular QAM due to its higher bandwidth efficiency [22]. An additional phase component is then added at one of the transmitters, which is used to carry additional information bits in the form of an M-ary phase shifting keying (MPSK) signal. For higher order MPSK, labeling diversity is then also applied to the phase component. At high SNR, the proposed system retains the error performance of a conventional USTLD system while improving spectral efficiency without an increase in power or bandwidth cost.

Rest of the paper is as follows: In section 2.1, the system model for USTLD is presented. In section 2.2, a low complexity (LC) detection scheme based on maximum likelihood (ML) detection is proposed. In section 2.3, a complexity analysis is performed comparing ML detection to the proposed LC detection. In section 2.4, the theoretical average bit error probability (ABEP) using a union bound approach is shown. In section 2.5, mapper design criterion and the mappers for XQAM and MPSK constellations is presented. In section 3, simulation results are presented and compared with the theoretical bound, and in section 4, this paper is concluded.

2 Labeling diversity with XQAM and MPSK modulation

2.1 System Model

A USTLD MIMO system is considered in this paper, with $N_T = 2$ transmit antennas, N_R receive antennas and $t = 4$ transmission timeslots, as shown in Fig. C.1 below.

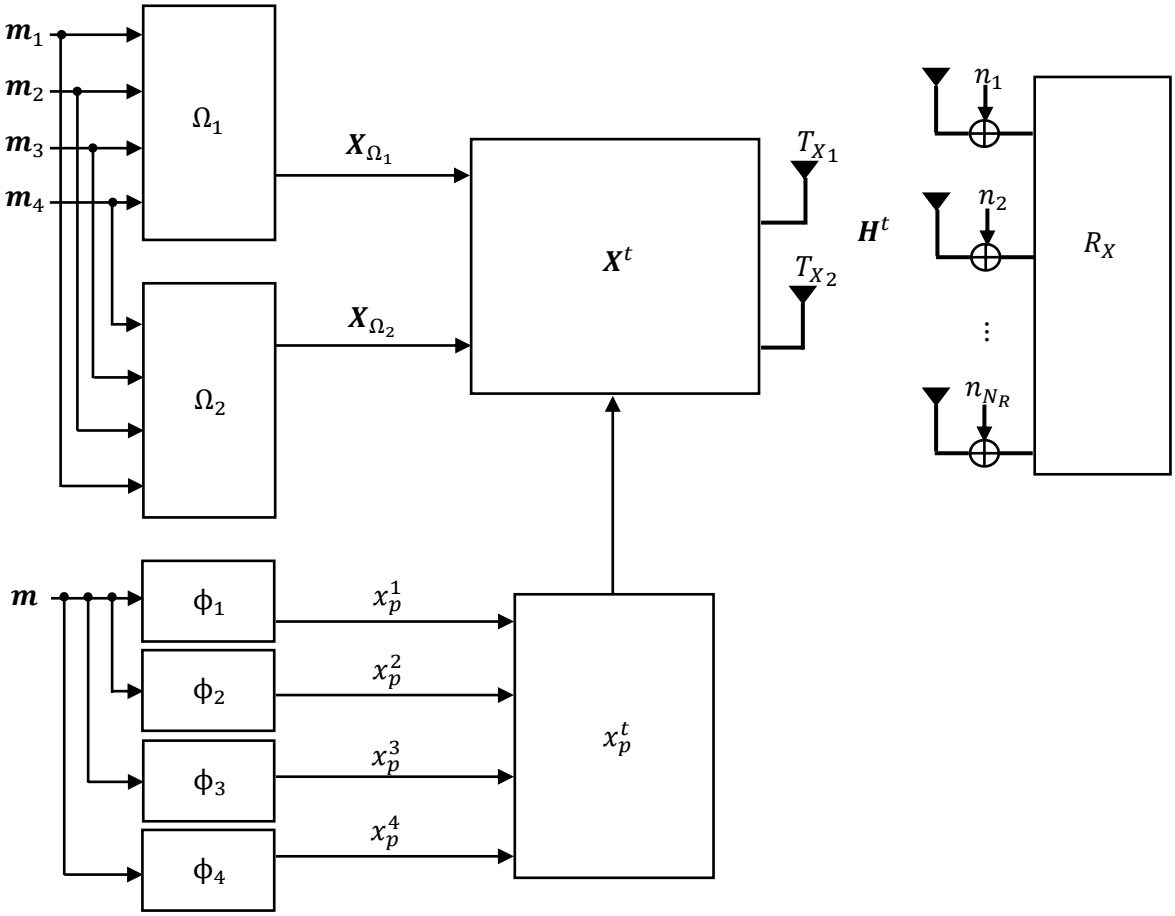

Fig. C.1 USTLD XQAM with MPSK system model

In Fig. C.1 $r_1 = \log_2 M_1$ and $r_2 = \log_2 M_2$, where M_1 is the constellation size of XQAM with $M_1 \in [32, 128]$ and M_2 is the constellation size of MPSK with $M_2 \in [4, 8, 16]$. A message of length $(4r_1 + r_2)$ is divided into vectors $\boldsymbol{m}_i = [m_{i,1}\, m_{i,2} \cdots m_{i,r_1}]$, $i \in [1:4]$ and $\boldsymbol{m} = [m_1\, m_2 \cdots m_{r_2}]$. Vectors $\boldsymbol{m}_i$, $i \in [1:4]$ are fed through Mappers Ω_k, $k \in [1:2]$ resulting in the XQAM symbols $x_{q_i}^k = \Omega_k(\boldsymbol{m}_i)$, where $q_i = 1 + \sum_{j=1}^{r_1} 2^{j-1} m_{i,j}$ is the index for the set of symbols $x_{q_i}^k$, $k \in [1:2]$. Vector $\boldsymbol{m}$ is fed through Mappers ϕ_k, $k \in [1:l]$, where l depends on the modulation order and labeling diversity of PSK. For 4PSK, there is no labeling diversity for the MPSK symbols, thus only one mapper is used. For 8PSK symbols, two mappers are used, whilst for 16PSK, four mappers are used. In the proposed system $l = 1, 2 \text{ and } 4$ for 4PSK, 8PSK

and 16PSK, respectively. Let $x_p^k = \phi_k(\boldsymbol{m}),\ k \in [1:l]$, where $p = 1 + \sum_{j=1}^{r_2} 2^{j-1} m_j$ is the index for the set of symbols $x_p^k,\ k \in [1:l]$. It is assumed that $E\left\{\left|x_{q_i}^k\right|^2\right\} = 1,\ i \in [1:4],\ k \in [1:2]$ and $E\left\{\left|x_p^k\right|^2\right\} = 1,\ k \in [1:l]$. Ω_1 maps the input bit stream using a Grey-coded XQAM constellation whilst ϕ_1 maps the input bit stream using a Grey-coded MPSK constellation. The designs for Ω_2 and $\phi_k,\ k \in [2:l]$, are based on optimizing the performance of the labeling diversity scheme, and its details can be found in section 2.5. The channel is assumed to experience Rayleigh frequency-flat fast fading. For the case of quasi-static fading, $\boldsymbol{h}_{2i-1,N_T} = \boldsymbol{h}_{2i,N_T},\ i \in [1:2],\ N_t \in [1:2]$. In Fig. C.1, $\boldsymbol{X}_{\Omega_1} = \left[x_{q_t}^1\ x_{q_{t+1}}^1\right],\ t \in [1,3]$, $\boldsymbol{X}_{\Omega_2} = \left[x_{q_t}^2\ x_{q_{t-1}}^2\right],\ t \in [2,4]$, $\boldsymbol{X}^t = \left[x_{q_t}^u \quad x_{q_{t+v}}^u x_p^t\right],\ t \in [1:4]$ and $\boldsymbol{H}^t = \begin{bmatrix}\boldsymbol{h}_{t,1}\\ \boldsymbol{h}_{t,2}\end{bmatrix},\ t \in [1:4]$.

The received signal for timeslot $t, t \in [1:4]$ is given by

$$\boldsymbol{y}_t = \sqrt{\frac{\rho}{2}}\left(\boldsymbol{h}_{t,1} x_{q_t}^u + \boldsymbol{h}_{t,2} x_{q_{t+v}}^u x_{p,t}\right) + \boldsymbol{n}_t \qquad t \in [1:4] \tag{C.1}$$

where $u = 1, v = 1$ for $t \in [1,3]$ and $u = 2, v = -1$ for $t \in [2,4]$. $\boldsymbol{y}_t = \left[y_{1,t}\ y_{2.t} \ldots\ y_{N_R.t}\right]^T$ is the received signal for timeslot t, and $\frac{\rho}{2}$ is the average signal-to-noise ratio (SNR) at each receive antenna. $x_{p,t}$ is the transmitted MPSK symbol for timeslot t, given by $\left[x_{p,1}\ x_{p,2}\ x_{p,3}\ x_{p,4}\right] = \begin{cases}\left[x_p^1\ x_p^1\ x_p^1\ x_p^1\right], & \text{4PSK}\\ \left[x_p^1\ x_p^1\ x_p^2\ x_p^2\right], & \text{8PSK}\\ \left[x_p^1\ x_p^2\ x_p^3\ x_p^4\right], & \text{16PSK}\end{cases}$, $\boldsymbol{h}_{t,i}$ is the fading channel of transmit antenna $i,\ i \in \{1:2\}$ for timeslot $t, t \in \{1:4\}$, where $\boldsymbol{h}_{t,i} = \left[h_{t,i}^1\ h_{t,i}^2 \cdots h_{t,i}^{N_R}\right]^T$ and $\boldsymbol{n}_t = [n_t^1\ n_t^2 \cdots n_t^{N_R}]^T$ is the additive white Gaussian noise (AWGN) noise vector. The entries for $\boldsymbol{h}_{t,1}, \boldsymbol{h}_{t,2}$ and $\boldsymbol{n}_t$ are independent and identically distributed (IID) according to the complex Gaussian distribution with $CN(0,1)$.

2.2 Detection schemes

It is assumed that the channel state information is fully known at the receive side. The optimal detection scheme is the maximum likelihood (ML) detection, given by

$$[\hat{q}_1\ \hat{q}_2\ \hat{q}_3\ \hat{q}_4\ \hat{p}\ ] = \underset{\substack{q_i \in [1:M_1], i \in [1:4]\\ p \in [1:M_2]}}{\operatorname{argmin}} \left[\sum_{t=1}^{4} \left\| \boldsymbol{y}_t - \sqrt{\frac{\rho}{2}}\left(\boldsymbol{h}_{t,1} x_{q_t}^u + \boldsymbol{h}_{t,2} x_{q_{t+v}}^u x_{p,t}\right)\right\|_F^2\right] \tag{C.2}$$

where $u = 1, v = 1$ for $t \in [1,3]$ and $u = 2, v = -1$ for $t \in [2,4]$

The ML detection in (C.2) for the proposed system would have very high complexity. In order to reduce the detection complexity, an alternate low complexity scheme based on ML detection is proposed in this section. The proposed scheme is based on the following observations:

- The MPSK symbols $x_{p,t},\ t \in [1:4]$ all have the same index, p. Therefore, knowledge of the index p implies knowledge of the MPSK symbols.
- If the index p of the MPSK symbol is known, the XQAM symbol indices $q_i,\ i \in [1,2]$ can be detected independently of the indices $q_i,\ i \in [3,4]$.

The proposed scheme works in two steps.

Step 1: Estimate the indices of the XQAM symbols $\hat{q}_i,\ i \in [1:2]$ and $\hat{q}_i,\ i \in [3:4]$ for a given MPSK symbol index $p,\ p \in [1:M_2]$ independently.

$$[\hat{q}_1(p)\ \ \hat{q}_2(p)\ \Upsilon_1(p)\ ] = \underset{\substack{q_i \in [1:M_1] \\ i \in [1:2]}}{\operatorname{argmin}} \left[\sum_{t=1}^{2} \left\| \boldsymbol{y}_t - \sqrt{\frac{\rho}{2}} \left(\boldsymbol{h}_{t,1} x_{q_t}^{u} + \boldsymbol{h}_{t,2} x_{q_{t+v}}^{u} x_{p,t} \right) \right\|_F^2 \right] \qquad (\text{C.3.1})$$

where $u = 1, v = 1$ for $t = 1$ and $u = 2\ , v = -1$ for $t = 2$.

$$[\hat{q}_3(p)\ \hat{q}_4(p)\ \ \Upsilon_2(p)\ ] = \underset{\substack{q_i \in [1:M_1] \\ i \in [3:4]}}{\operatorname{argmin}} \left[\sum_{t=3}^{4} \left\| \boldsymbol{y}_t - \sqrt{\frac{\rho}{2}} \left(\boldsymbol{h}_{t,1} x_{q_t}^{u} + \boldsymbol{h}_{t,2} x_{q_{t+v}}^{u} x_{p,t} \right) \right\|_F^2 \right] \qquad (\text{C.3.2})$$

where $u = 1, v = 1$ for $t = 3$ and $u = 2\ , v = -1$ for $t = 4$

In the above detection, the outputs $\hat{q}_i(p),\ i \in [1:4]$ are the estimated indices for the transmitted q_i given the index p of the MPSK symbol. $\Upsilon_k(p), k \in [1:2]$ is the ML detection metric for jointly detecting q_{2k-1} and q_{2k}.

Step 2: estimate the index of the MPSK symbol.

Let $\boldsymbol{\Upsilon} = \left[\left(\Upsilon_1(1) + \Upsilon_2(1) \right) \left(\Upsilon_1(2) + \Upsilon_2(2) \right)\ \cdots\ \left(\Upsilon_1(M_2) + \Upsilon_2(M_2) \right) \right]$. The estimated index of the MPSK symbol is given by

$$\left[\left(\Upsilon_1(\hat{p}) + \Upsilon_2(\hat{p}) \right)\ \hat{p} \right] = \operatorname{argmin}\ (\boldsymbol{\Upsilon}\ ) \qquad (\text{C.4})$$

where $\hat{p}$ is the index corresponding to the minimum element $\left(\Upsilon_1(\hat{p}) + \Upsilon_2(\hat{p}) \right)$ of $\boldsymbol{\Upsilon}$.

Finally, the detected XQAM indices are given by

$$\hat{q}_i\ = \hat{q}_i(\hat{p}) \qquad i \in\ [1:4] \qquad (\text{C.5})$$

2.3 Receiver complexity analysis and comparison

In order to compare the computational complexity of ML detection and the proposed low complexity (LC) detection, we analyse both schemes in terms of the number of complex operations required.

Computational complexity for ML detection

For ML detection, we analyse (2). The terms $\boldsymbol{h}_{t,1}x_{q_t}^{u}$ and $\boldsymbol{h}_{t,2}x_{q_{t+v}}^{u}x_{p,t}$ require N_R complex operations. Summing the terms and subtracting from $\boldsymbol{y}_t$ each requires N_R complex operations. Finally, the Frobenius norm operation requires N_R complex operations. As there are a total of 4 timeslots, the computational complexity for the argument in (2) is $4 \times 5N_R = 20N_R$. Therefore, the total complexity for ML detection is $20(M_1)^4 M_2 N_R$.

Computational complexity for LC detection

For LC detection, we analyse (3.1), (3.2) and (3.3). Following a similar procedure as detailed for (2) above, it can be shown that the complexity for the arguments of (3.1) and (3.2) are both $10N_R$. The computational complexity for (4) is equal to $M_2 - 1$ real operations, which is equivalent to $\frac{M_2-1}{4}$ complex operations. Thus, the total complexity for LC detection is $20(M_1)^2 M_2 N_R + \frac{M_2-1}{4}$.

The table below shows the percentage reduction in complexity achieved by LC detection over ML detection for $M_1 \in [32, 128]$, $M_2 \in [4, 8, 16]$ and $N_R = 4$.

Table 3 Complexity reduction for LC detection vs ML detection

$\boldsymbol{M_1}$	$\boldsymbol{M_2}$	Complexity reduction (%)
32	4	99.9%
32	8	99.9%
32	16	99.9%
128	4	99.9%
128	8	99.9%
128	16	99.9%

Clearly, a significant reduction in complexity is achieved using LC detection; approximately a factor of $(M_1)^2$.

2.4 Performance analysis for USTLD using union bound approach

The error performance analysis for USTLD with square MQAM has been discussed in [10], where it was assumed that at high SNR, only one symbol is detected in error. We extend that approach in the proposed system to assume that at high SNR, during each transmission block of four timeslots, only one type of information symbol is detected in error, either XQAM symbols (symbol error) or MPSK symbol (phase error). Further, it is assumed that for symbol error, only one of the symbols is detected with error. For the convenience of this discussion it is assumed that $x_{q_1}^k$ is detected with error while $x_{q_i}^k,\ i \in [2:4]$ are detected correctly. Based on these assumptions, the equivalent system model for phase error becomes

$$\boldsymbol{y}_t = \sqrt{\frac{\rho}{2}}\widetilde{\boldsymbol{h}}_t x_{p,t} + \boldsymbol{n}_t, \qquad t \in [1:4] \tag{C.6}$$

where $\left[\widetilde{\boldsymbol{h}}_1\ \widetilde{\boldsymbol{h}}_2\ \widetilde{\boldsymbol{h}}_3\ \widetilde{\boldsymbol{h}}_4\right] = \left[\boldsymbol{h}_{1,2}x_{q_2}^1\ \boldsymbol{h}_{2,2}x_{q_1}^2\ \ \boldsymbol{h}_{3,2}x_{q_4}^1\ \ \boldsymbol{h}_{4,2}x_{q_3}^2\right]$

For symbol error, the equivalent system model is

$$\boldsymbol{y}_t = \sqrt{\frac{\rho}{2}}\boldsymbol{h}_{t,t}x_{q_1}^t + \boldsymbol{n}_t, \qquad t \in [1:2] \tag{C.7}$$

Let P_s be the symbol error probability and P_θ be the phase error probability. Based on the above assumptions, the overall bit error probability P_e is bounded by

$$P_e = 1 - \mathrm{P_c} = P_s + P_\theta - P_s P_\theta \leq P_s + P_\theta \tag{C.8}$$

where $P_c = (1 - P_s)(1 - P_\theta)$ is the probability all bits are detected correctly. From (C.6-C.8), the ABEP for XQAM USTLD with MPSK is

$$ABEP(\rho) \leq \frac{1}{M_1 r_1}\sum_{q_1,=1}^{M_1}\sum_{\hat{q}_1 \neq q_1}^{M_1} N_1(q_1, \hat{q}_1)\, P\left(\boldsymbol{X}_{q_1} \to \boldsymbol{X}_{\hat{q}_1}\right) + \frac{1}{M_2 r_2}\sum_{p=1}^{M_2}\sum_{\hat{p} \neq p}^{M_2} N_2(p, \hat{p})\, P\left(\boldsymbol{X}_p \to \boldsymbol{X}_{\hat{p}}\right) \tag{C.9}$$

where $P\left(\boldsymbol{X}_{q_1} \to \boldsymbol{X}_{\hat{q}_1}\right)$ is the pairwise error probability (PEP) that the transmitted XQAM codeword $\boldsymbol{X}_{q_1}$ is detected as $\boldsymbol{X}_{\hat{q}_1}$ where $\boldsymbol{X}_{q_1} = \left[x_{q_1}^1\ x_{q_1}^2\right]$ and $\boldsymbol{X}_{\hat{q}_1} = \left[x_{\hat{q}_1}^1\ x_{\hat{q}_1}^2\right]$. $P\left(\boldsymbol{X}_p \to \boldsymbol{X}_{\hat{p}}\right)$ is the PEP that the transmitted MPSK codeword $\boldsymbol{X}_p$ is detected as $\boldsymbol{X}_{\hat{p}}$ where $\boldsymbol{X}_p = \left[x_{p,1}\ x_{p,2}\ x_{p,3}\ x_{p,4}\right]$ and $\boldsymbol{X}_{\hat{p}} = \left[x_{\hat{p},1}\ x_{\hat{p},2}\ x_{\hat{p},3}\ x_{\hat{p},4}\right]$. $N_1(q_1, \hat{q}_1)$ and $N_2(p, \hat{p})$ are the number of bit errors for the associated PEP events.

Based on the equivalent model (C.6), the conditional PEP for phase error can be expressed as

$$P\left(\boldsymbol{X}_p \to \boldsymbol{X}_{\hat{p}} |\, \boldsymbol{h}_{1,2}, \cdots, \boldsymbol{h}_{4,2}\right) = P\left(\sum_{t=1}^{4} \left\|\boldsymbol{y}_t - \widetilde{\mathbf{H}}_t x_{\hat{p},t}\right\|_F^2 < \sum_{t=1}^{4} \left\|\boldsymbol{y}_t - \widetilde{\mathbf{H}}_t x_{p,t}\right\|_F^2\right) \quad \text{(C. 10)}$$

where $\widetilde{\mathbf{H}}_t = \sqrt{\frac{\rho}{2}}\widetilde{\boldsymbol{h}}_{\boldsymbol{t}}$. This can be further expressed as:

$$P\left(\boldsymbol{X}_p \to \boldsymbol{X}_{\hat{p}} |\, \boldsymbol{h}_{1,2}, \ldots, \boldsymbol{h}_{4,2}\right) = Q\left(\sqrt{\frac{1}{2}\sum_{t=1}^{4} \delta_t}\right) \quad \text{(C. 11)}$$

where $\delta_t = \left\|\widetilde{\mathbf{H}}_t \Lambda_t\right\|_F^2$ and $\Lambda_t = x_{p,t} - x_{\hat{p},t},\ t \in \{1..4\}$. The derivation of (C.11) is shown in the Appendix. The PDF of δ_t is [24, eq. 2-1-110]

$$f_{\delta_t}(v_t) = \frac{v_t^{N_R-1}}{\left(\frac{\rho}{4}|\Lambda_t|^2\right)^{N_R}(N_R-1)!} \exp\left(-\frac{v_t}{\frac{\rho}{4}|\Lambda_t|^2}\right) \quad \text{(C. 12)}$$

Averaging the conditional PEP over the independent and identically distributed (IID) random variables, the PEP can be expressed as:

$$P\left(\boldsymbol{X}_p \to \boldsymbol{X}_{\hat{p}}\right) = \int_0^\infty \int_0^\infty \int_0^\infty \int_0^\infty P\left(\boldsymbol{X}_p \to \boldsymbol{X}_{\hat{p}} |\, \boldsymbol{h}_{1,2}, \ldots, \boldsymbol{h}_{4,2}\right) \prod_{t=1}^{4} f_{\delta_t}(v_t) dv_t \quad \text{(C. 13)}$$

By approximating the Q-function using the trapezoidal rule, the PEP can be expressed as

$$P\left(\boldsymbol{X}_p \to \boldsymbol{X}_{\hat{p}}\right) = \frac{1}{2n}\left[\frac{1}{2}\prod_{t=1}^{4} M_t\left(\frac{1}{2}\right) + \sum_{k=1}^{n-1}\prod_{t=1}^{4} M_t\left(\frac{1}{2\sin^2\left(\frac{k\pi}{2n}\right)}\right)\right] \quad \text{(C. 14)}$$

where the approximation is convergent when number of summations $n > 10$, and $M_t(s)$ is the moment generating function of δ_t given by

$$M_t(s) = \int_0^\infty f_{\delta_t}(v_t)\, e^{-sv_t} dv_t = \left(\frac{1}{1+\frac{\rho}{4}|\Lambda_t|^2 s}\right)^{N_R} \quad \text{(C. 15)}$$

Finally, substituting (C.15) into (C.14):

$$P\left(\boldsymbol{X}_p \to \boldsymbol{X}_{\hat{p}}\right) = \frac{1}{2n}\left[\frac{1}{2}\prod_{t=1}^{4}\left(1+\frac{\rho}{8}|\Lambda_t|^2\right)^{-N_R} + \sum_{k=1}^{n-1}\prod_{t=1}^{4}\left(1+\frac{\rho}{8}|\Lambda_t|^2\frac{1}{\sin^2\left(\frac{k\pi}{2n}\right)}\right)^{-N_R}\right] \quad \text{(C. 16)}$$

Based on the equivalent model (C.7), the conditional PEP for symbol error can be expressed as

$$P\left(\boldsymbol{X}_{q_1} \to \boldsymbol{X}_{\hat{q}_1} | \boldsymbol{h}_{1,1}, \boldsymbol{h}_{2,2}\right) = P\left(\sum_{t=1}^{2} \left\|\boldsymbol{y}_t - \mathbf{H}_{\mathrm{t,t}} x_{\hat{q}_1}^t\right\|_F^2 < \sum_{t=1}^{2} \left\|\boldsymbol{y}_t - \mathbf{H}_{\mathrm{t,t}} x_{q_1}^t\right\|_F^2\right) \quad \text{(C. 17)}$$

where $\mathbf{H}_{\mathrm{t,t}} = \sqrt{\frac{\rho}{2}}\boldsymbol{h}_{t,t}$. Similar to the derivation of the PEP for phase error, the conditional PEP for symbol error can be further derived as

$$P\left(\boldsymbol{X}_{q_1} \to \boldsymbol{X}_{\hat{q}_1} | \boldsymbol{h}_{1,1}, \boldsymbol{h}_{2,2}\right) = Q\left(\sqrt{\frac{1}{2}\kappa}\right) \tag{C. 18}$$

where $\kappa = \left\|\mathbf{H}_{1,1} d_1\right\|_F^2 + \left\|\mathbf{H}_{2,2} d_2\right\|_F^2$ and $d_i = x_{q_1}^i - x_{\hat{q}_1}^i, \ \ i \in [1{:}\,2]$. This is equivalent to [10, eq. 15]. Following the same approach as [10], the PEP can be shown as [10, eq. 10]

$$P\left(\boldsymbol{X}_{q_1} \to \boldsymbol{X}_{\hat{q}_1}\right) = \frac{1}{2n}\left[\frac{1}{2}\prod_{i=1}^{2}\left(1 + \frac{\rho}{8}|d_i|^2\right)^{-N_R} + \sum_{k=1}^{n-1}\prod_{i=1}^{2}\left(1 + \frac{\rho}{8}|d_i|^2 \frac{1}{\sin^2\left(\frac{k\pi}{2n}\right)}\right)^{-N_R}\right] \tag{C. 19}$$

2.5 Mapper design for USTLD XQAM and MPSK constellation

At high SNR, $|d_i|^2 \gg 1, \ i \in [1{:}\,2]$ and $|\Lambda_t|^2 \gg 1, \ t \in [1{:}\,4]$, (C.16) and (C.19) respectively can be approximated as

$$P\left(\boldsymbol{X}_{q_1} \to \boldsymbol{X}_{\hat{q}_1}\right) = \frac{1}{2}\prod_{i=1}^{2}\left(\frac{\rho}{8}\,|d_i|^2\right)^{-N_R} + \sum_{k=1}^{n-1}\prod_{i=1}^{2}\left(\frac{\rho}{8}\,|d_i|^2 \frac{1}{\sin^2\left(\frac{k\pi}{2n}\right)}\right)^{-N_R} \tag{C. 20.1}$$

$$P\left(\boldsymbol{X}_{p} \to \boldsymbol{X}_{\hat{p}}\right) = \frac{1}{2}\prod_{t=1}^{4}\left(\frac{\rho}{8}|\Lambda_t|^2\right)^{-N_R} + \sum_{k=1}^{n-1}\prod_{t=1}^{4}\left(\frac{\rho}{8}|\Lambda_t|^2 \frac{1}{\sin^2\left(\frac{k\pi}{2n}\right)}\right)^{-N_R} \tag{C. 20.2}$$

From inspecting (C.20), the design criterion in [10] can also be applied to designing both XQAM and MPSK mappers, which was shown to be maximizing of the minimum product distance (PD), given by

$$\Omega_2 = \underset{q_1 \in [1:\mathrm{M}_1]}{\operatorname{argmax}}\left\{\underset{(\hat{q}_1 \neq q_1) \in [1:M_1]}{\operatorname{argmin}} \prod\nolimits_{k=1}^{2} |d_k|^2\right\} \tag{C. 21.1}$$

$$(\phi_2, \ldots, \phi_{\mathrm{j}}) = \underset{p \in [1:M_2]}{\operatorname{argmax}}\left\{\underset{(\hat{p} \neq p) \in [1:M_2]}{\operatorname{argmin}} \prod\nolimits_{t=1}^{4} |\Lambda_t|^2\right\} \tag{C. 21.2}$$

where $j = 2$ for 8PSK, $j = 4$ for 16PSK.

Since it is not practical to compute (C.21.1) and (C.21.2) directly [7, 8], a few different approaches are used for the design of the mappers. For 32XQAM and 128XQAM, the method proposed in [10] for MQAM is used: Adjacent constellation points in Mapper 1 are placed away

from each other in Mapper 2 by grouping alternate diagonal pairs in each quadrant and then swapping them with diagonal pairs in the diagonally opposite quadrant. This is visualized in Figure 7.1 in the Appendix: In the top left quadrant, the diagonals formed by the constellation points 1A and 2A are swapped with the diagonals in the bottom right quadrant formed by the points 1B and 2B respectively. Similarly, in the bottom left quadrant, the diagonals formed by 3A, 4A and 5A swapped with the diagonals in the top right quadrant formed by 3B, 4B and 5B, respectively. For 8PSK, the approach shown in [10, Fig. 1] is used: alternate diagonal constellation points are swapped. For 16PSK, since 4 mappers are used, the optimal symbol mappings for 16PSK proposed in [7] are used. The full symbol mappings for each mapper are shown in the appendix.

3 Simulation Results

Monte Carlo simulations of the USTLD system for 32QAM and 128QAM with 4PSK, 8PSK and 16PSK using the mappers described above were performed, with the results shown in Fig. C.2 and C.3 respectively. For reference, simulation results for the performance of USTLD for XQAM without MPSK is shown, and the theoretical result using the union bound approach is included. $N_r = 4$ receivers were used. It was assumed that channel information was known at the receive side, and the channel fading was fast.

It can be seen that the theoretical bound provides a close match to the simulation results at high SNR (>13dB). At low SNR, the addition of MPSK to the USTLD system degrades performance, but at high SNR, the performance converges. An XQAM USTLD system with 16PSK results in a bit rate improvement of 20% for 32QAM and 14.3% for 128QAM. In Fig.C.4-C.7, performance of USTLD for 32QAM and 128QAM with 16PSK is compared with Alamouti for both fast and quasi-static fading channels. The results show that at high SNR, USTLD shows significantly better performance than Alamouti, with a coding gain of 2dB for quasi-static fading and 3dB for fast fading.

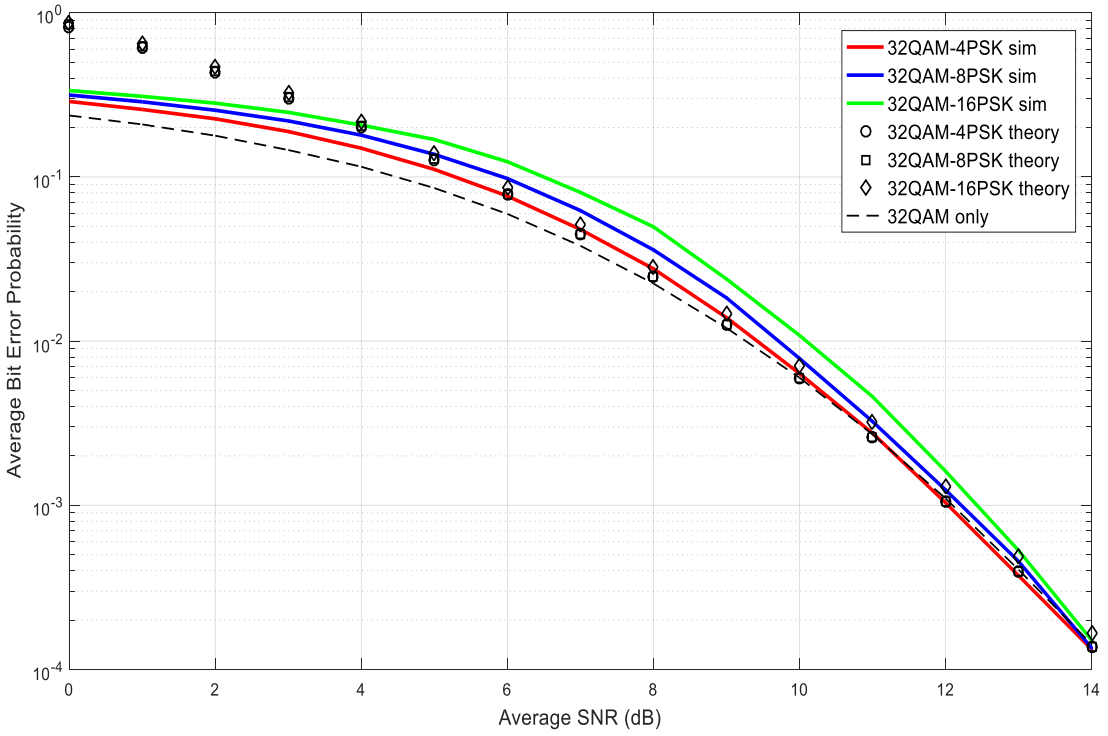

Fig. C.2 32XQAM USTLD with MPSK

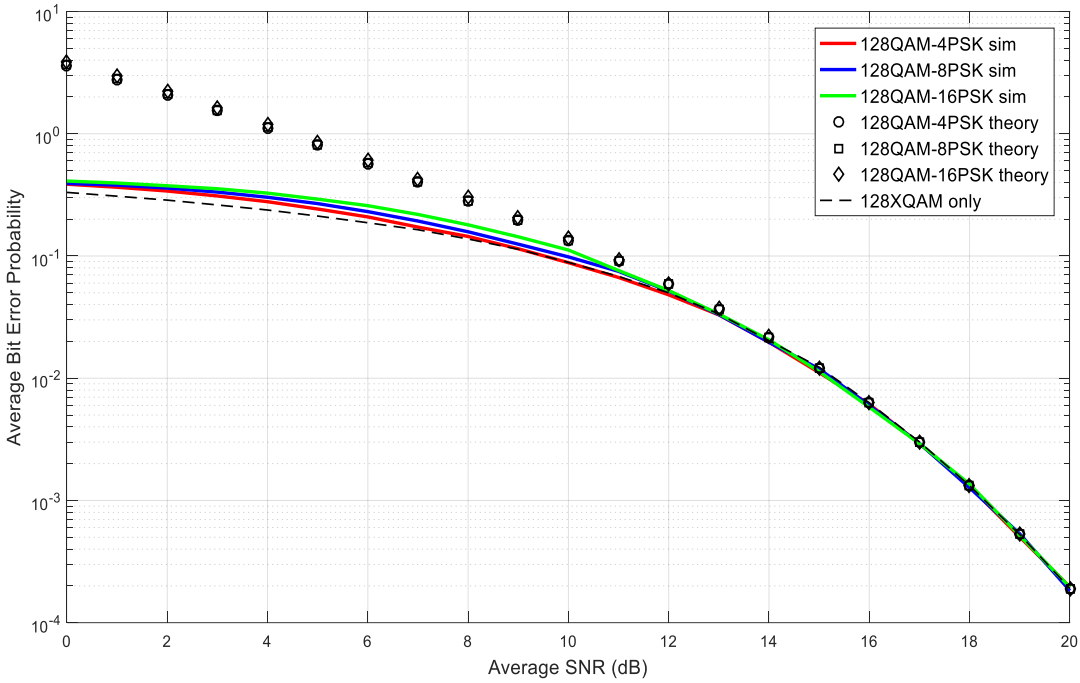

Fig. C.3 128XQAM USTLD with MPSK

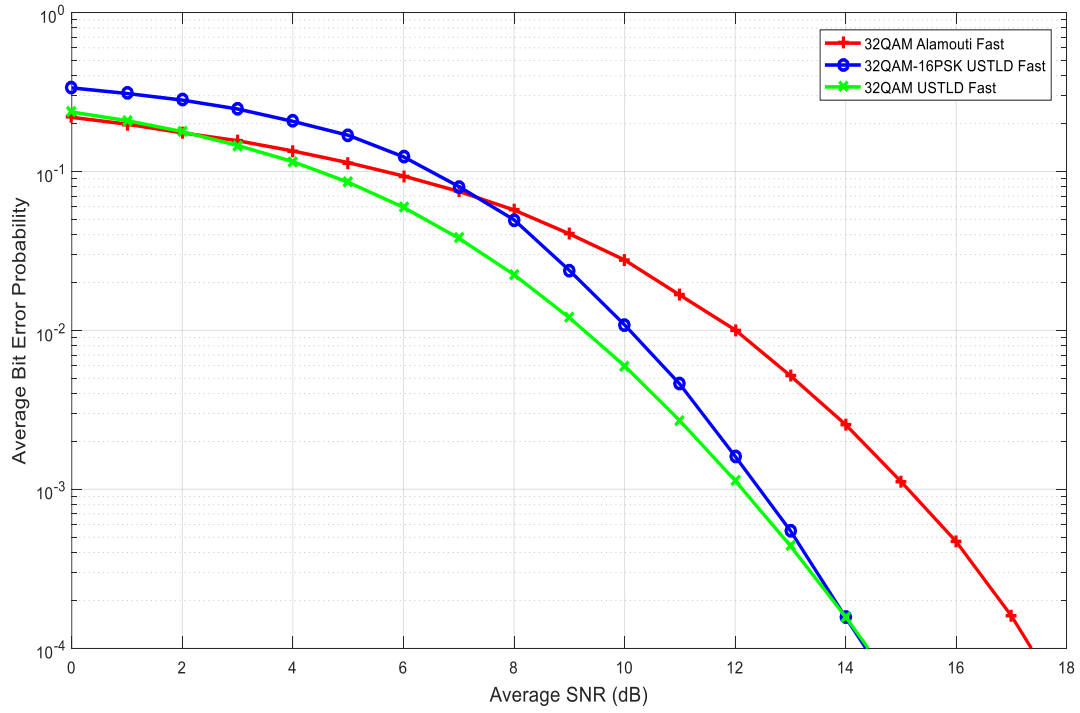

Fig. C.4 32XQAM USTLD vs Alamouti, fast fading

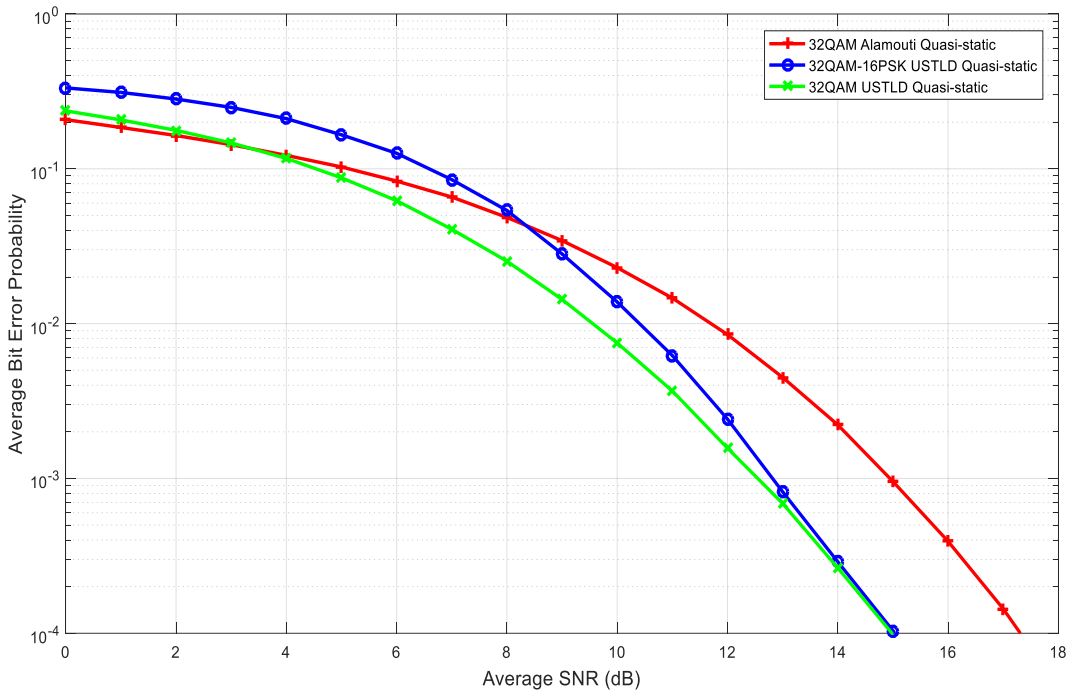

Fig. C.5 32XQAM USTLD vs Alamouti, quasi-static fading

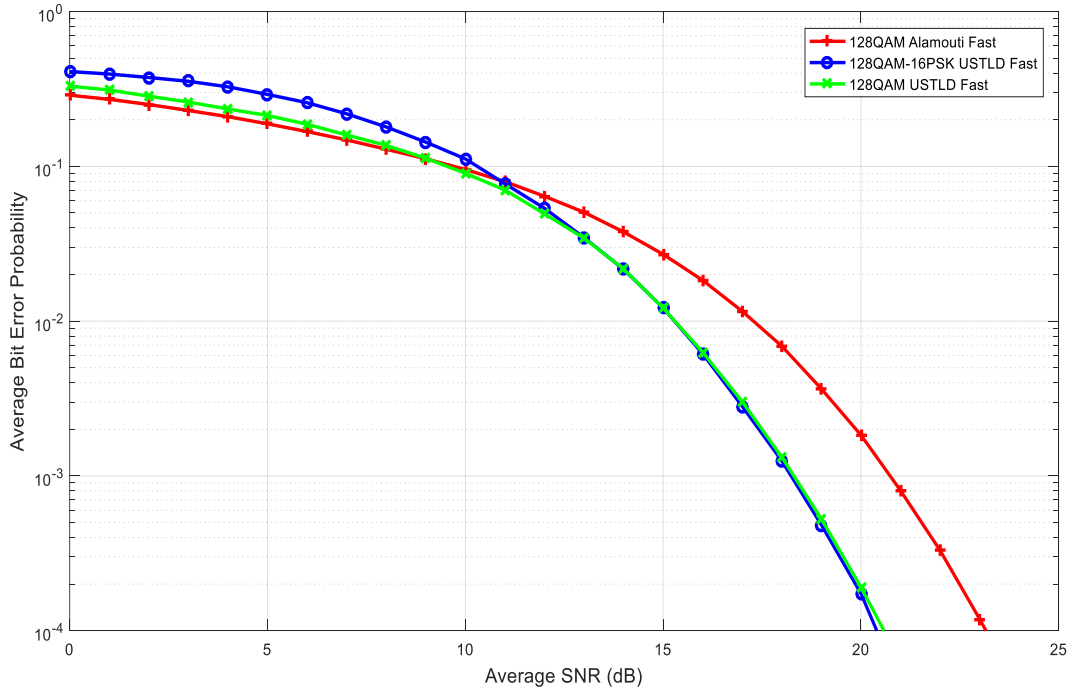

Fig. C.6 128XQAM USTLD vs Alamouti, fast fading

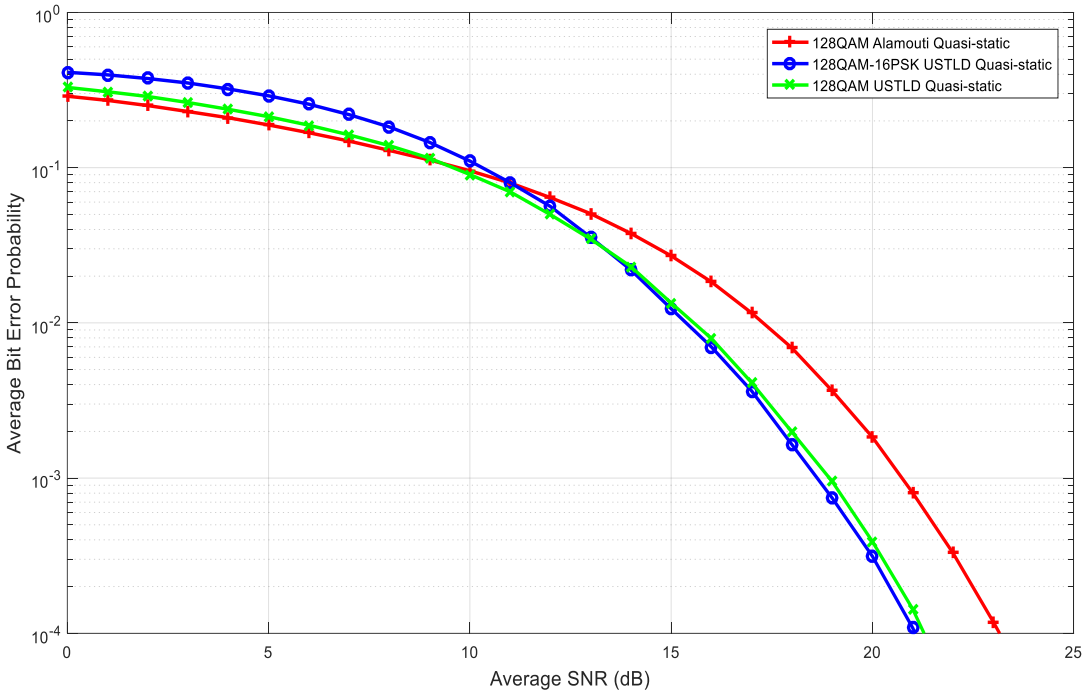

Fig. C.7 128XQAM USTLD vs Alamouti, quasi-static fading

4 Conclusion

In this paper, a USTLD system has been designed for XQAM modulation with MPSK. The theoretical ABEP is analysed using a union bound and is shown to provide a close match to simulation results at high SNR. Criteria for optimal mapper design and a few simple approaches are followed to generate the various mappers used in the proposed system. These results allow the application of USTLD systems with higher spectral efficiency than previously proposed USTLD systems by adding an MPSK phase rotation.

5 Appendix

Substituting $\boldsymbol{y}_t$ from (C.6) and expanding yields

$$P\left(\boldsymbol{X}_p \to \boldsymbol{X}_{\hat{p}} | \, \boldsymbol{h}_{1,2}, \dots, \boldsymbol{h}_{4,2}\right) = P\left(\sum_{t=1}^{4}\left[\left\|\widetilde{\mathbf{H}}_t \Lambda_t\right\|_F^2 + 2Re\{\Lambda_t \boldsymbol{n}_t^H \widetilde{\mathbf{H}}_t\}\right] < 0\right) \quad \text{(C. 22)}$$

$$P\left(\boldsymbol{X}_p \to \boldsymbol{X}_{\hat{p}} | \, \boldsymbol{h}_{1,2}, \dots, \boldsymbol{h}_{4,2}\right) = P\left(\sum_{t=1}^{4}\left[Re\{\Lambda_t \boldsymbol{n}_t^H \widetilde{\mathbf{H}}_t\}\right] > \frac{1}{2}\sum_{t=1}^{4}\left\|\widetilde{\mathbf{H}}_t \Lambda_t\right\|_F^2\right) \quad \text{(C. 23)}$$

$\Lambda_t \boldsymbol{n}_t^H \widetilde{\mathbf{H}}_t$, $t \in [1{:}\,4]$ are complex Gaussian random variables with zero mean and variance of $\left\|\Lambda_t \widetilde{\mathbf{H}}_t\right\|_F^2$.

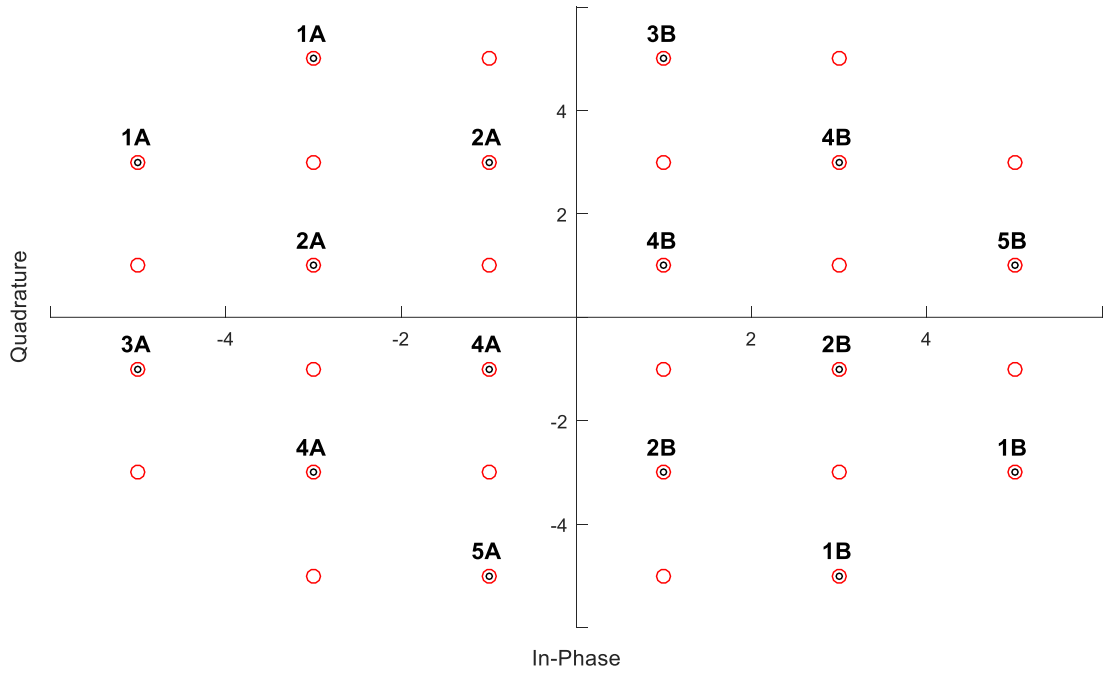

Fig. C.8 32XQAM diagonal groupings

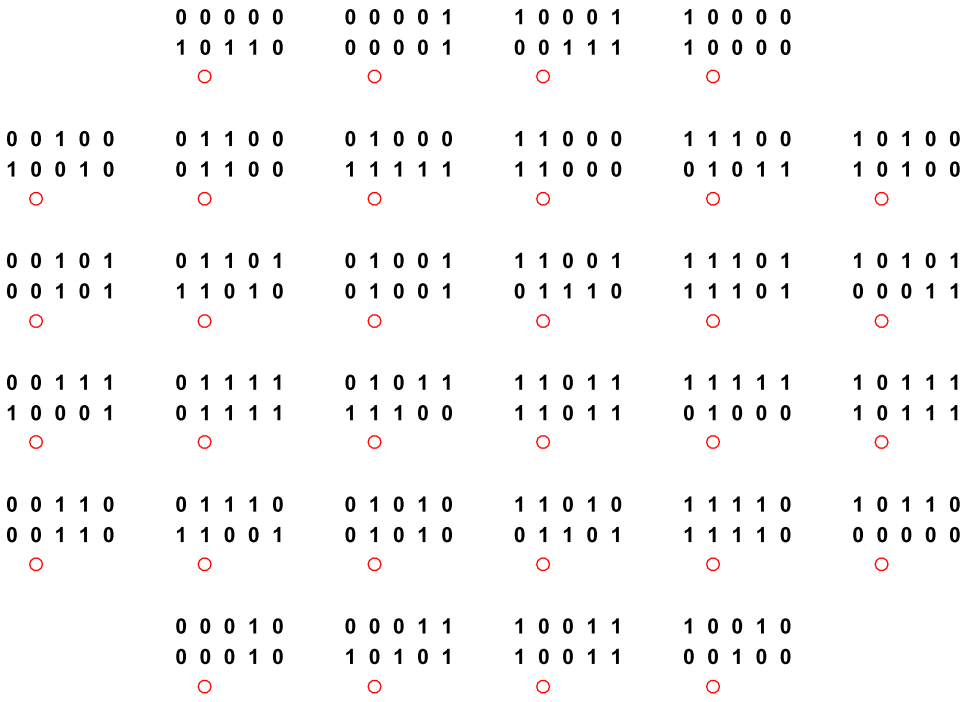

Fig. C.9 32XQAM symbol mappings

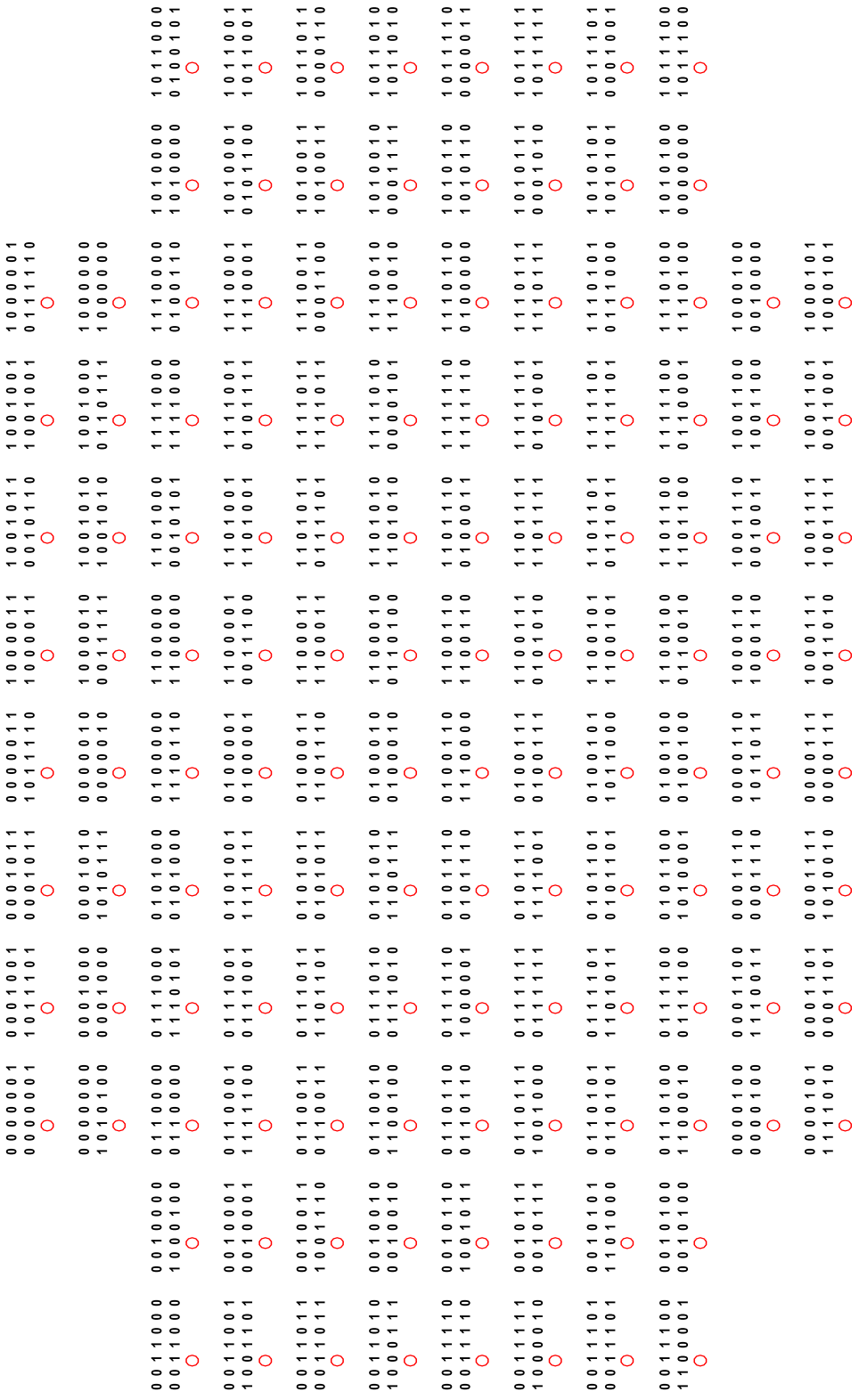

Fig. C.10 128XQAM Mappings

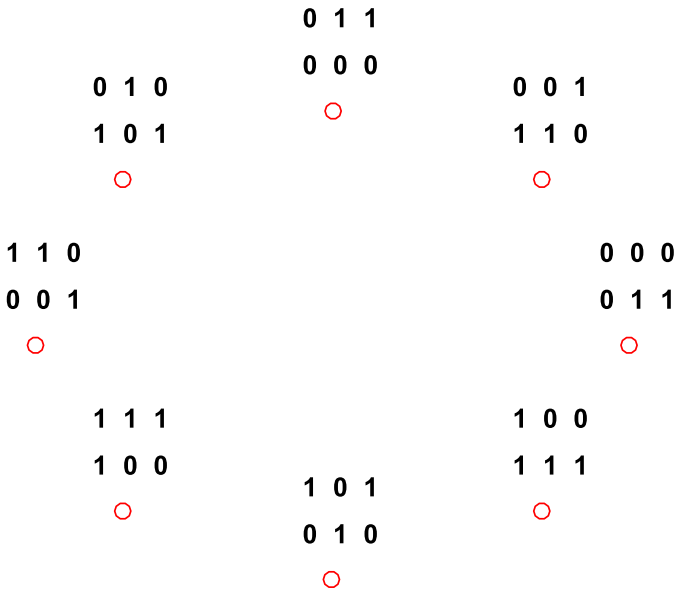

Fig. C.11 8PSK Mappings

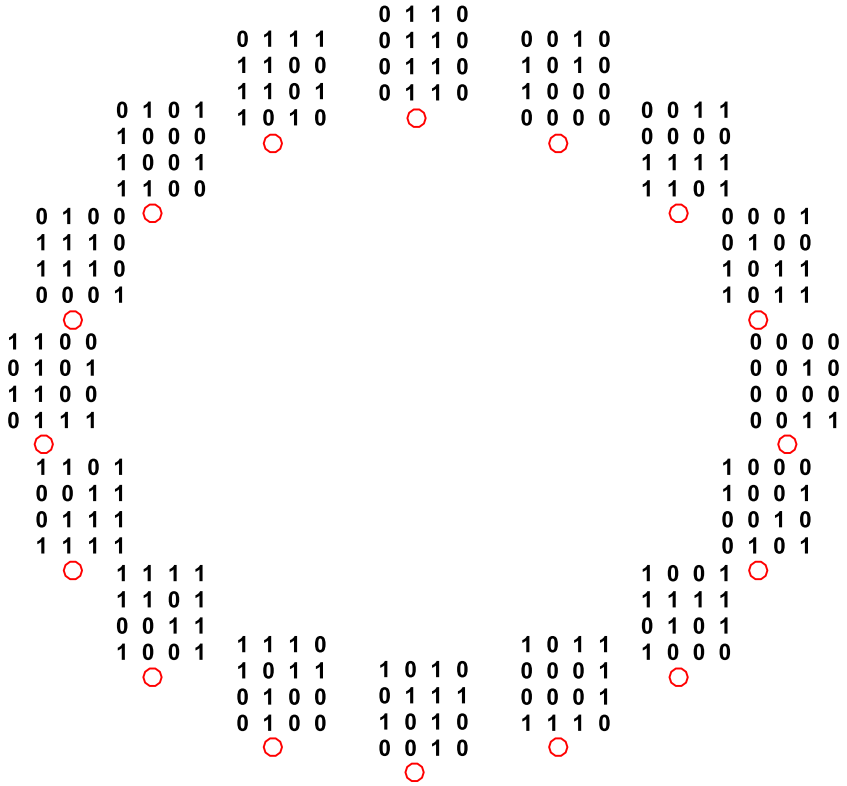

Fig. C.12 16PSK Mappings

6 References

[1] X. Li, A. Chindapol and J. Ritcey, "Bit-interleaved coded modulation with iterative decoding and 8 PSK signaling," *IEEE Trans. on Commun.,* vol. 50, no. 8, pp. 1250-1257, Aug. 2002.

[2] A. Chindapol and J. Ritcey, "Design, analysis, and performance evaluation for BICM-ID with square QAM constellations in Rayleigh fading channels," *IEEE J. Sel. Areas Commun.,* vol. 19, no. 5, pp. 944-957, May 2001.

[3] Y. Huang and J. Ritcey, "Optimal constellation labeling for iteratively decoded bit-interleaved space-time coded modulation," *IEEE Trans. Inf. Theory,* vol. 51, no. 5, pp. 1865-1871, May 2005.

[4] Y. Huang and J. Ritcey, "Improved 16-QAM constellation labeling for BI-STCM-ID with the Alamouti scheme," *IEEE Comm. Lett.,* vol. 9, no. 2, pp. 157-159, Feb. 2005.

[5] M. Krasicki, "Improved labelling diversity for iteratively-decoded multi-antenna systems," in *Proc. 7th IWCMC*, Istanbul, Jul. 2011.

[6] M. Krasicki, "Essence of 16-QAM labelling diversity," *Electron. Lett.,* vol. 49, no. 8, pp. 567-569, Apr. 2013.

[7] H. Samra, Z. Ding and P. Hahn, "Symbol mapping diversity design for multiple packet transmissions," *IEEE Trans. on Commun.,* vol. 53, no. 5, pp. 810-817, May 2005.

[8] K. Seddik, A. Ibrahim and K. Liu, "Trans-modulation in wireless relay networks," *IEEE Comm. Lett.,* vol. 12, no. 3, pp. 170-172, Mar. 2008.

[9] "Enhanced HARQ Method with Signal Constellation Rearrangement," Panasonic, Las Vegas, Mar. 2001.

[10] H. Xu, K. Govindasamy and N. Pillay, "Uncoded space-time labeling diversity," *IEEE Commun. Lett.,* vol. 20, no. 8, pp. 1511-1514, Jun. 2016.

[11] D. Ayanda, H. Xu and N. Pillay, "Uncoded M-ary Quadrature Amplitude Modulation Space-time Labeling diversity with three transmit antennas," *IJCS.*

[12] K. Govindasamy, H. Xu and N. Pillay, "Space-Time Block Coded Spatial Modulation with Labeling Diversity," *IJCS,* vol. 31, no. 1, Jan. 2018.

[13] T. Quazi and H. Xu, "SSD-Enhanced Uncoded Space-Time Labeling Diversity," *IJCS,* vol. 31, no. 11, Jul. 2018.

[14] S. Patel, T. Quazi and H. Xu, "Error Performance of Uncoded Space Time Labeling Diversity in Spatially Correlated Nakagami-q Channels," *IJCS,* vol. 31, no. 12, Aug. 2018.

[15] Q. Ling and T. Li, "Efficiency Improvement for Alamouti Codes," in *IEEE CISS*, Princeton, NJ, Mar. 2006.

[16] R. Vishwanath and M. Bhatnagar, "High Data Rate Alamouti Code From Field Extension," *Wireless Personal Comms,* vol. 40, no. 4, pp. 489-494, Jun. 2006.

[17] S. Das, N. Al-Dhahir and R. Calderbank, "Novel Full-Diversity High-Rate STBC for 2 and 4 Transmit Antennas," *IEEE Commun.,* vol. 10, no. 3, pp. 171-173, Jun. 2006.

[18] M. Sinnokrot, J. Barry and V. Madisetti, "Embedded Alamouti Space-Time Block Codes for High Rate and Low Decoding Complexity," in *IEEE CSSC*, Asilomar, 2008.

[19] X. Li and L. Wang, "High Rate Space-Time Block Coded Spatial Modulation with Cyclic Structure," *IEEE Commun. Lett.,* vol. 18, no. 4, pp. 532-535, Apr. 2014.

[20] A. Helmy, M. Di Renzo and N. Al-Dhahir, "Enhanced-Reliability Cyclic Generalized Spatial-and-Temporal Modulation," *IEEE Commun. Lett.,* vol. 20, no. 12, pp. 2374-2377, Dec. 2016.

[21] B. Dlodlo and H. Xu, "Trellis Code-Aided High-Rate M-QAM Space-Time Labeling Diversity Using a Unitary Expansion," *IJCS,* vol. 31, no. 8, Jun. 2018.

[22] J. Smith, "Odd-bit quadrature amplitude-shift keying," *IEEE Trans. on Commun.,* vol. 23, no. 3, pp. 385-389, 1975.

[23] J. Proakis, Digital Communications, New York, USA: McGraw-Hill, 2001.

Part 3

Conclusion

Conclusion

In the first two papers presented, SEP performance analysis for SIMO systems using XQAM modulation and MRC diversity reception was performed. The trapezoidal rule was used to provide a tight approximation for the Gaussian Q-function and alternative Q-function, respectively. Closed-form expressions for the SEP over fading channels were then derived by using the MGF form of the fading channel PDFs. Paper A considered dual-correlated, identically distributed channels, while paper B considered an arbitrary number of non-identical, correlated channels with known channel covariance matrix.

These results allow for simple numerical analysis of the aforementioned systems, with expressions that provide a tight approximation to the expected results, and aid in the design and tuning of XQAM systems experiencing correlated channel behavior.

Paper C presented a USTLD system for XQAM modulation with an added MPSK phase rotation. Choosing 16PSK allows for a bit rate improvement of 20% for 32QAM and 14.3% for 128QAM. Criteria for optimal signal mapper design guided the design approach for finding mappers for both XQAM and MPSK constellations. The results from this paper can be generalized to provide designs for any USTLD system employing an odd-bit transmission scheme. The proposed scheme can be of use in systems requiring a higher spectral efficiency than that offered by a standard USTLD system.

In general, the results of this thesis provide further insight into the design and performance of XQAM systems, and provide the tools necessary to predict system behavior without the need for extensive simulations.